

Grand Unification of Solutions of Accretion and Winds around Black Holes and Neutron Stars

Sandip K. Chakrabarti¹

Goddard Space Flight Center, Greenbelt MD, 20771

and Tata Institute of Fundamental Research, Homi Bhabha Road, Bombay, 400005²

e-mail: I: chakraba@tifrvax.tifr.res.in

: Submitted June 7th, 1995; Appearing in ApJ on June 20th, 1996.

Received _____; accepted _____

ABSTRACT

We provide the complete set of global solutions of viscous transonic flows (VTFs) around black holes and neutron stars. These solutions describe the optically thick and optically thin flows from the horizon of the black hole or from the neutron star surface to the location where the flow joins with a Keplerian disk. We study the nature of the multiple sonic points as functions of advection, rotation, viscosity, heating and cooling. Stable shock waves, which join two transonic solutions, are found to be present in a large region of the parameter space. We classify the solutions in terms of whether or not the flow can have a standing shock wave. We find no new topology of solutions other than what are observed in our previous studies of isothermal VTFs. We particularly stress the importance of the boundary conditions and argue that we have the most complete solution of accretion and winds around black holes and neutron stars.

Subject headings: accretion, accretion disks — black hole physics — stars:
neutron – stars: mass loss — hydrodynamics – shock waves

¹ NRC Senior Research Associate at GSFC

² Permanent Address

1. INTRODUCTION

Standard accretion disk models of Shakura & Sunyaev (1973; hereafter SS73) and Novikov & Thorne (1973) have been very useful in interpretation of observations in binary systems and active galaxies (e.g. Pringle 1981; Shapiro & Teukolsky, 1984; Frank et al., 1992). The description of physical quantities in these models are expressed analytically and they could be used directly. However, these models do not treat the pressure and advection terms correctly, since the disk is terminated at the marginally stable orbit (three Schwarzschild radii for a non-rotating black hole) and no attempt was made to satisfy the inner boundary condition on the horizon. A second problem arose, when it was pointed out (Lightman & Eardley, 1974) that the inner regions of these disks are viscously and thermally unstable. Observationally, there are overwhelming evidences that the disks are *not* entirely Keplerian (see, Chakrabarti 1993, 1994, 1995, 1996, hereafter C93; C94; C95; and C96 respectively). The soft and high states of the galactic and extragalactic black hole candidates (Tanaka et al., 1989; Ebisawa et al., 1994) are very poorly understood, and it has been suggested very recently (Chakrabarti & Titarchuk 1995, hereafter CT95) that this change of states could be attributed to the presence of the sub-Keplerian components which may include shock waves. The general agreements of the prediction of CT95 with observations strongly suggest the reality of sub-Keplerian advective flow models.

Paczyński and his collaborators (Paczyński & Bisnovatyi-Kogan, 1980; Paczyński & Muchotrzeb, 1982) have attempted to include advection and pressure effects in the so-called transonic accretion disks, although no systematic study of global solutions were performed. Global solutions of the so-called ‘thick accretion disks’ were possible to obtain only when the advection term is dropped (e.g., Paczyński & Wiita, 1980). In these accretion disks, the flow is assumed to have practically constant angular momentum. Some exact solutions of fully general relativistic thick disks are discussed in Chakrabarti (1985; hereafter C85).

Early attempts to find global solutions of viscous transonic flow (VTF) equations (Muchotrzeb, 1983; Matsumoto et al. 1984) concentrated much on the nature of the inner sonic point of these flows which is located around the marginally stable orbit. In the case of inviscid adiabatic flow, an example of global solution was provided by Fukue (1987) who performed a study of shocks similar to that in solar winds and galactic jets (e.g., Ferrari et al., 1985) and found evidence of shock transition as well. In the so-called ‘slim-disk’ model of Abramowicz et al. (1988), it was tried to show from *local solutions* that the instabilities at the inner edge could be removed by addition of the advection term (see, a similar trial by Taam & Fryxall, 1985; Chakrabarti, Jin & Arnett, 1987, where thermonuclear reaction in the disk was used to eliminate the instability). The global solution of Abramowicz et al. was not completely satisfactory to the present author, since the angular momentum, instead of joining to Keplerian, *deviated away* from it close to the outer edge (see, Fig. 3 of Abramowicz et al. 1988). First satisfactory global solution of these equations in the optically thin or thick limit which include advection, viscosity, heating and cooling in the limit of isothermality condition was obtained by Chakrabarti (1990a, hereafter C90a; 1990b, hereafter C90b) where disk models of (single) temperature ($\gtrsim 1.e + 11K$) which become Keplerian far away were considered. Recent self-consistent Comptonization work of CT95 shows that in the presence of soft-photon source from Keplerian component, the protons can be isothermal (see, Fig. 2 of CT95) in some range of accretion rates ($\sim 0.3 - 0.5$ times the Eddington rate) and therefore isothermality condition of C90a,b may be more realistic than thought before.

In an earlier work (Chakrabarti 1989, hereafter C89), we have presented the complete classification of global solutions of an *inviscid*, polytropic transonic flow (see, Fig. 4 of C89) which showed that in some region of the parameter space, the flow will have multiple sonic points (e.g., Liang & Thomson, 1980). We also found that within this region, there is a sub-class of solutions where Rankine-Hugoniot shock conditions are satisfied and shock

waves are formed due to the centrifugal barrier (centrifugally supported shocks). These shock solutions are perfectly transonic. Matter inflowing into a black hole crosses a sonic region three times, twice (continuously) at the outer and the inner sonic points, and once (discontinuously) at the shock location. Four locations, namely, x_{si} , ($i = 1..4$) were identified where these shocks could formally be located, but it was pointed out that only x_{s2} and x_{s3} were important for accretion on black holes since the flow has to be supersonic on a black hole horizon and x_{s1} could also be important for a neutron star accretion while x_{s4} was a purely formal shock location. In Chakrabarti 90a, and 90b, viscosity was also added and complete global solutions in isothermal VTFs with and without shocks, were found. In the language of Shakura-Sunyaev (SS73) viscosity parameter α , it was shown that if viscosity parameter is less than some critical value α_{cr} , the incoming flow may either have a continuous solution passing through outer sonic point, or, it can have standing shock waves at x_{s3} or x_{s2} (following notations of C89 or C90a,b) if the flow allows such a solution in accretion. For $\alpha > \alpha_{cr}$, a standing shock wave at x_{s2} persisted, but the flow now had two continuous solutions — one passed through the inner sonic point, and the other through the outer sonic point. Later analytical and numerical works (Chakrabarti & Molteni, 1993, 1995; hereafter CM93 and CM95 respectively, Nobuta & Hanawa 1994, Nakayama 1992) showed that x_{s3} is stable, and that for $\alpha > \alpha_{cr}$ the continuous solution passing through the inner sonic point is chosen. We noted that α_{cr} (~ 0.015 for the isothermal case considered) was a function of the model parameters, such as the disk temperature, sonic point location and angular momentum on the horizon. Most importantly, these solutions show that they join with the Keplerian disks at some distance, depending upon viscosity and angular momentum (C90a, CM95). This discussion of critical α is valid when the inner sonic point and angular momentum of the flow at the inner edge is kept fixed (see below).

Extensive numerical simulations of quasi-spherical, inviscid, adiabatic accretion flows (Molteni, Lanzafame & Chakrabarti 1994; hereafter MLC94), show that shocks form very

close to the location where vertically averaged model of adiabatic flows predict them (C89). The flow advected its entire energy to the black hole and the entropy generated at the shock is also totally advected allowing the flow to pass through the inner sonic point. It was also found, exactly as predicted in C89, that flows with positive energy and higher entropy form strong, supersonic winds. In presence of viscosity also, very little energy radiates away (e.g., Fig. 8 of C90a). Having satisfied ourselves of the stability of these solutions (CM93, MLC94, CM95), we proposed a unified scheme of accretion disks (C93, C94; C96, and CM95) which combines the physics of formation of sub-Keplerian disks with and without shock waves depending on viscosity parameters and angular momentum at the inner edge. We always considered only the stable branch of VTF and our solutions remained equally valid for black hole and neutron star accretions as long as appropriate inner boundary conditions are employed. Importance of these findings are currently being reconsidered in the so-called ‘newly discovered advection dominated model’ (Narayan & Yi, 1994; see Narayan, 1996 and references therein).

In this paper, we make a comprehensive study of the global solutions of the VTF equations applicable to black hole and neutron star accretion. We remove the restriction of isothermality condition imposed in C90a and 90b, and made explicit use of the energy equation. We classify the solutions according to whether or not an accretion flow can have shock waves. We include the effects of advection, rotation, viscosity, heating and cooling as before. We discover the existence of two critical viscosity parameters: $\alpha_{c1}(x_{in}, l_{in})$ and $\alpha_{c2}(x_{in}, l_{in})$ which control the nature of the inner regions of the disk (Here, x_{in} and l_{in} denote the inner sonic point and the angular momentum of the flow on the horizon or star surface respectively.) Out of these two, α_{c2} has the same meaning (shock/no-shock) as α_{cr} in isothermal case (C90a) whereas α_{c1} (also present in isothermal case, but we did not explore it before) determines whether the flow would be in the accretion shock regime in the first place. We assume the standard viscosity type prescription (SS73), but the viscous

stress is assumed to be proportional to the thermal pressure (standard assumption of SS73) or the total (thermal plus ram) pressure (CM95). The latter is useful when advection (radial velocity) is important. We also examine the effects of the polytropic index of the flow on the sonic point behavior and note that typically, for $\gamma \lesssim 1.5$ there are multiple sonic points (see, Fig 3.1 of C90b). For $\gamma \gtrsim 1.5$, or generally for higher viscosity or lower cooling efficiency the outer saddle type sonic points are absent and therefore shocks could only form if the flow is already supersonic (such as coming from some stellar winds). In all these cases, even with general heating and cooling, we do not discover any new topologies other than what are already discovered in C90a and C90b. We argue in Section 5 that there should not be any new topologies either. We therefore believe that the present result contains the most complete solutions to date which one may have around a black hole or a neutron star. We do not consider accretion through nodal points (Matsumoto et al., 1984) as the stability properties of these solutions are uncertain.

Throughout the paper, we give importance to two fundamental issues related to a black hole and neutron star accretion: the nature of the sonic points, and the typical distances (x_{Kep}) at which the disk may join a Keplerian disk. Understanding of the nature of the sonic point is important, since matter accreting on a black hole must pass through it (C90b). Similarly, knowledge of how x_{Kep} depends on viscosity is very crucial because of the possible role it may have on the observed high energy phenomena, such as novae outbursts and soft and high states of galactic black hole candidates. The spectra would be a mixture of the emission from Keplerian and non-Keplerian components (CT95) and we need to know at what distance the deviation from Keplerian distribution becomes important. These non-Keplerian flows have been exactly solved using the sonic point analysis and their properties studied extensively in the past few years using restricted equation of states (C89, C90a, C90b). In the present paper, we only extend these studies to include more general heating and cooling processes. Non-axisymmetric, non-Keplerian, vertically averaged flows

which are more difficult to deal with have been solved using self-similarity assumption (Chakrabarti 1990c; see also Spruit, 1987 who used self-similarity for a disk of constant height or conical disk without vertical averaging.) with polytropic equation of state. These studies in the present context of more general heating and cooling will be presented in future.

In our analysis of black hole and neutron star accretion, we use the Paczyński-Wiita (1980) potential. This potential is known to mimic the geometry around a Schwarzschild black hole quite satisfactorily and is widely used in the astrophysical community. One major misgivings of our present work may be that we do not use general relativity (GR). Our prior experience of solving inviscid disks in Kerr geometry (Chakrabarti, 1990d) indicates that no new topological properties emerge when full general relativity is used. Even in magnetohydrodynamical studies (Takahashi et al., 1990; Englemaier, 1993) no new topology emerges other than what is observed with pseudo-Newtonian potential (Chakrabarti, 1990e). The generalized equations in Kerr geometry using the prescription of Novikov & Thorne (1973), but with conserved angular momentum $l = -u_\phi/u_t$, do not yield any new topologies either (Chakrabarti, 1996b). Only quantitative change is the possible reversal of shear stress just outside the horizon (Anderson & Lemos, 1988). In GR one could apply the inner boundary condition (‘lock-in’ of the flow with the horizon) rigorously than what we could do with pseudo-Potential. For instance, the definition of angular velocity of matter is related to the angular momentum (Ω) by (e.g., C85):

$$\Omega = \frac{l}{\lambda^2}$$

where,

$$\lambda^2 = -\frac{u_\phi u^t}{u_t u^\phi} = \frac{x^2 \sin^2 \theta}{1 - \frac{1}{x}}$$

(The second equality is valid for Schwarzschild geometry. Here, u^μ s are the four velocity components and l is the specific angular momentum.) Thus, by definition, independent of

how much angular momentum is carried in by the flow, the flow would have ‘zero’ angular velocity on the horizon ($x = 1$). However, when using a pseudo-potential, this condition is not met: $\Omega = l_{in}/x^2$ is a Newtonian definition (l_{in} being the angular momentum of the inflow on the horizon) and it does not vanish at $x = 1$, the horizon (here distance x is measured in units of $x_g = 2GM_{BH}/c^2$). Usually this poses no threat. The potential energy is infinite at $x = 1$ in this potential, hence, the rotational energy term $\Omega^2 x^2/2$ is always insignificant at $x = 1$. The same consideration of ‘locking-in’ condition for a Kerr black hole implies that the rotational velocity of the flow ‘matches’ with that of the black hole at the horizon (e.g., Novikov & Thorne, 1973). A pseudo-potential has been constructed with this consideration (Chakrabarti & Khanna, 1992) which is valid for small Kerr parameter ‘a’ only. For a neutron star solution, the situation is simpler: one just has to choose the final subsonic branch such that on the star surface, $x = R_*$, $\Omega_* R_*^2 = l_{in}$ condition is satisfied. In the numerical simulations (CM93, MLC94, CM95) the inner boundary condition is achieved by putting an ‘absorption’ boundary condition at $x \sim 1$.

The plan of the paper is the following: in the next section, we present model equations, description of each terms and show why such flows would have multiple sonic points. In §3, we present analytical solutions for flow parameters at the sonic points using both the viscosity prescriptions. In §4, we present results depicting extensively how the solution topologies depend on the disk parameters. In §5, we briefly argue about the completeness of our solutions. Finally, in §6, we make concluding remarks.

2. MODEL EQUATIONS

We assume units of length, velocity and time to be $x_g = 2GM_{BH}/c^2$, c and $2GM_{BH}/c^3$ respectively. We assume the flow to be vertically averaged. Comparison of numerical

simulations of thick accretion (MLC94) with analytical results (C89) indicate that vertically averaged treatments are basically adequate. The equations of motion which we employ (CT95, C96) are similar to, but not exactly same as those used by Paczyński & Bisnovatyi-Kogan, 1981; Matsumoto et al. 1984; Abramowicz et al. 1988; C90a,b; Narayan & Yi, 1994. We use,

(a) The radial momentum equation:

$$\vartheta \frac{d\vartheta}{dx} + \frac{1}{\rho} \frac{dP}{dx} + \frac{l_{Kep}^2 - l^2}{x^3} = 0, \quad (1a)$$

(b) The continuity equation:

$$\frac{d}{dx}(\Sigma x \vartheta) = 0, \quad (1b)$$

(c) The azimuthal momentum equation:

$$\vartheta \frac{dl(x)}{dx} - \frac{1}{\Sigma x} \frac{d}{dx}(x^2 W_{x\phi}) = 0, \quad (1c)$$

(d) The entropy equation:

$$\Sigma \vartheta T \frac{ds}{dx} = \frac{h(x)\vartheta}{\Gamma_3 - 1} \left(\frac{dP}{dx} - \Gamma_1 \frac{P}{\rho} \frac{d\rho}{dx} \right) = Q^+ - Q^- = \alpha q^+ - g(x, \dot{M}) q^+ = f(\alpha, x, \dot{M}) Q^+, \quad (1d)$$

where,

$$\Gamma_3 = 1 + \frac{\Gamma_1 - \beta}{4 - 3\beta},$$

$$\Gamma_1 = \beta + \frac{(4 - 3\beta)^2(\gamma - 1)}{\beta + 12(\gamma - 1)(1 - \beta)}$$

and $\beta(x)$ is the ratio of gas pressure to total pressure,

$$\beta = \frac{\frac{\rho k T}{\mu m_p}}{\frac{1}{3} \bar{a} T^4 + \frac{\rho k T}{\mu m_p}}.$$

Here, \bar{a} is the Stefan constant, k is the Boltzman constant, m_p is the mass of the proton and μ is the mean molecular weight. Note that for a radiation dominated flow, $\beta \sim 0$, and $\Gamma_1 = 4/3 = \Gamma_3$ and for a gas pressure dominated flow, $\beta \sim 1$, and $\Gamma_1 = \gamma = \Gamma_3$. Using the above definitions, eqn. (1d) becomes,

$$\frac{4 - 3\beta}{\Gamma_1 - \beta} \left[\frac{1}{T} \frac{dT}{dx} - \frac{1}{\beta} \frac{d\beta}{dx} - \frac{\Gamma_1 - 1}{\rho} \frac{d\rho}{dx} \right] = f(\alpha, x, \dot{M}) Q^+. \quad (1e)$$

In this paper, we shall concentrate on solutions with constant β . Actually we study in detail only the special cases, $\beta = 0$ and $\beta = 1$, so we shall liberally use $\Gamma_1 = \gamma = \Gamma_3$. Similarly, we shall consider the case for $f(\alpha, x, \dot{M}) = \text{constant}$, though as is clear, $f \sim 0$ in the Keplerian disk region and probably closer to or less than 1 near the black hole depending on the efficiency of cooling (governed by \dot{M} , for instance). If the cooling process is ‘super-efficient’, namely, when the flow cools faster than it is heated, f could be negative as well. Two examples of global solutions with such a possibility, one with bremsstrahlung cooling in weak viscosity limit (Molteni, Sponholz, & Chakrabarti, 1996; hereafter MSC96) and the other with Comptonization (CT95) have been recently discussed. Results of the general equation (1e) will be presented in near future. We use Paczyński-Wiita (1980) potential to describe the black hole geometry. Thus, l_{Kep} , the Keplerian angular momentum is given by, $l_{Kep}^2 = x^3/2(x-1)^2$. Here, $W_{x\phi}$ is the vertically integrated viscous stress, $h(x)$ is the half-thickness of the disk at radial distance x obtained from vertical equilibrium assumption (C89), $l(x)$ is the specific angular momentum, ϑ is the radial velocity, s is the entropy density of the flow, Q^+ and Q^- are the heat gained and lost by the flow, and \dot{M} is the mass accretion rate. The constant α above is the Shakura-Sunyaev (SS73) viscosity parameter which defines the viscous stress as $W_{x\phi} = -\alpha W = -\alpha_P W$, where W is the

integrated pressure P . (We shall refer to this $W_{x\phi}$ as the “P-stress” in future.) As noted earlier (CM95), instead of having the stress proportional to the thermal pressure W as in SS73 it is probably more appropriate to use $W_{x\phi} = -\alpha\Pi = -\alpha_{\Pi}\Pi$ while studying flows with significant radial velocity, since, especially, the total pressure (or, the momentum flux) $\Pi = W + \Sigma\vartheta^2$ is continuous across the shock and such a $W_{x\phi}$ keeps the angular momentum across of the shock to be continuous as well. (We shall refer to this $W_{x\phi}$ as the “ Π -stress” in future.) Except for eq. 1d, other equations are the same as used in our previous studies (C89 and C90ab). The term $g(x, \dot{M}) \leq \alpha$ is a dimensionless proportionality constant, which will be termed as the cooling parameter. When $g \rightarrow \alpha$, the flow is efficiently cooled, but when $g \rightarrow 0$, the flow is heating dominated and most *inefficiently* cooled. In C89, eq. 1d was replaced by the adiabatic equation of state $P = K\rho^\gamma$ with entropy constant K different in pre-shock and post-shock flows, and in C90a, eqn. 1d was replaced by the isothermal equation of state $W = K^2\Sigma$ (K being the sound speed of the gas and Σ being the integrated density of matter). In the present paper, for simplicity, we assume $f(\alpha, x, \dot{M}) = (\alpha - g)/\alpha = \text{const}$. We have verified that our conclusions do not change when more general cooling laws are used instead. Details will be presented in future.

Though in computing angular momentum distribution, we talked about using the shear stress of the first (1) form, $W_{x\phi}(1) = -\alpha W$, we wish to note that a second (2) form, such as, $W_{x\phi}(2) = \eta x d\Omega/dx$ (e.g., C90a,b) is also used in the literature. However, the latter choice requires an extra boundary condition, which, in the context of Paczyński-Wiita (1980) potential is difficult to implement, since on the horizon, various physical quantities become singular. Thus, in some example of C90a,b, we chose $d\Omega/dx$ at the sonic point assuming angular momentum remains almost constant between the sonic point and the horizon. While computing the heating term,

$$Q^+ = W_{x\phi}^2/\eta$$

one could use either $W_{x\phi}(1)$, or , $W_{x\phi}(2)$ or a combination of both! If only $W_{x\phi}(1)$ is used, no information of ‘actual shear’ is present in the heating term. If only $W_{x\phi}(2)$ is used the equations become difficult to solve, as the sonic point condition does not remain algebraic any more. (This was not a problem in C90a and C90b; as the heating equation was replaced by isothermality condition.) In the present paper, we have chosen to use the combination of both forms in order that we may be able to do sonic point analysis with *local* quantities (Flammang, 1982) at the same time retaining the memory of $d\Omega/dx$ of the flow. We call this prescription as the MIXed Shear Stress (MISStress) prescription. Roughly speaking, this method is almost equivalent to replacing one factor of $d\Omega/dx$ by $d\Omega_{Kep}/dx$ while other factor of $d\Omega/dx$ is kept in tact. Satisfactory preliminary results with this are already reported in the Appendix of CT95 and C96. We have verified that the results with only $W_{x\phi}(1)$ are very similar.

In order to understand the origin of multiple sonic points, we consider the property of constant energy surfaces as in the phase-space analysis in classical mechanics. Integrating eq. (1a) for an isothermal flow ($\gamma = 1$), and ignoring resulting slowly varying logarithmic thermal energy term, we get the specific energy of the flow to be,

$$E = \frac{1}{2}\vartheta^2 + \frac{1}{2}\frac{l^2}{x^2} - \frac{1}{2(x-1)}.$$

Note that since the potential energy term (third term) is dominant compared to the rotational energy term (second term) both at a large distance $x \rightarrow \infty$ as well as close to the horizon $x \rightarrow 1$, the behavior of constant energy contours in the phase space ($\vartheta - x$ plane, or, equivalently, in $M - x$ plane for isothermal flows) is *hyperbolic* (because of the negative sign in front of $(x - 1)^{-1}$ term) and as a result, saddle type sonic point is formed. In the intermediate distance, $l \sim x$, the rotational term is dominant and the constant energy contours are elliptical (because of the positive sign in front of l^2/x^2 term) and center type sonic point is formed (C90b). Of course, whether or not all these three sonic points will

be present depends on the angular momentum, polytropic index γ , viscosity, heating and cooling effects.

From the continuity equation (1b), we obtain the mass accretion rate to be given by,

$$\dot{M} = 2\pi\rho h(x)\vartheta \quad (2)$$

and from the azimuthal momentum equation,

$$l - l_{in} = \frac{\alpha_P x}{\gamma} \frac{x}{\vartheta} a^2 \quad (3a)$$

(see C90a, C90b) using P-stress prescription: $W_{x\phi} = -\alpha_P W$, or,

$$l - l_{in} = \alpha_{\Pi} \frac{x}{\vartheta} a^2 \left[\frac{2}{3\gamma - 1} + M^2 \right] \quad (3b)$$

for the Π -stress prescription (CM95) $W_{x\phi} = -\alpha_{\Pi}(W + \Sigma\vartheta^2)$. Here $M = \vartheta/a$ is the Mach number of the flow, a being the sound speed (defined by $a^2 = \gamma P/\rho$). The thickness of the disk is $h(x) \sim ax^{1/2}(x-1)$. The integration constant l_{in} represents the angular momentum at $x = 1$ which we refer to as the specific angular momentum at the inner edge of the flow, namely on the horizon. For a neutron star accretion the inner boundary condition has to be $l_{in} = \Omega_* R_*^2$ at $x = R_*$ as discussed earlier. Since in the regime of the pseudo-Newtonian potential, $v \rightarrow \infty$ and a =finite on the horizon, this identification is justified. The derivation of the squared bracketed terms of eq. (3b) requires an understanding of the vertically averaged quantities (C89, Matsumoto et al. 1984),

$$\Sigma = \int_{-h/2}^{h/2} \rho dz = \rho_e I_n h \quad W = \int_{-h/2}^{h/2} p_e I_{n+1} h = p_e I_{n+1} h \quad (4)$$

where, ρ_e , and p_e are the equatorial quantities. In terms of $n = 1/\gamma - 1$, I_n is given by,

$$I_n = \frac{(2^n n)^2}{(2n + 1)}. \quad (5)$$

Below, we present results using both the P-stress and Π -stress prescriptions. Though generally results are similar, angular momentum is found to be continuous across the shock

when we use Π -stress, whereas it is discontinuous when we use P-stress. Thus, the shock becomes purely compressible type when ram pressure is included in the stress, whereas it becomes a mixture of shear and compressible types when only thermal pressure is included (CM95). The other difference is that since there are two terms in Π -stress which come from the thermal and ram pressures, $\alpha_P \sim 2\alpha_\Pi$. We shall discuss both types of flows here for completeness, though we shall study examples of purely compressible shocks for simplicity using Π -stress.

3. SONIC POINT ANALYSIS

We solve equations 1(a)-1(e) using a sonic point analysis as before (C89, C90a,b).

3.1. Results Using “P-Stress”

This analysis is done with $W_{x\phi} = -\alpha_P W$. This is used in computing the angular momentum distribution (3a). However, in computing Q^+ , we have used MISStress prescription. Here, one has

$$Q^+ = \alpha_P h(x) x \frac{d\Omega}{dx}.$$

Hence eq. (1e) becomes,

$$\frac{2n}{a} \frac{da}{dx} - \frac{1}{\rho} \frac{d\rho}{dx} = \alpha_P f(\alpha, x, \dot{M}) \vartheta \frac{d\Omega}{dx}.$$

The function f will be close to zero in the Keplerian disk at the outer edge due to efficient cooling process and $f < 1$ close to the black hole (it could even be negative for super-cooled system, especially for weakly viscous case, either for optically thin flows with

bremsstrahlung emission, MSC96, or, for optically slim flows with Comptonization process, CT95). But we choose it to be a constant for simplicity, and also for clarity we use α in stead of α_P in the rest of this section. After some algebra we find,

$$\frac{d\vartheta}{dx} = \frac{N}{D}, \quad (6)$$

where the numerator is,

$$N = \left[\frac{1}{2(x-1)^2} - \frac{l^2}{x^3} - \frac{a^2}{\gamma} \frac{5x-3}{2x(x-1)} \right] \left[\frac{(2n+1)\gamma}{a^2} - \frac{2\alpha^2 f}{\vartheta^2} \right] - \left[\frac{5x-3}{2x(x-1)} + \frac{2l\alpha f}{\vartheta x^2} - \frac{\alpha^2 f a^2}{\gamma x \vartheta^2} \right] \quad (7a)$$

and the denominator is,

$$D = \left[\frac{(2n+1)\gamma}{a^2} - \frac{2\alpha^2 f}{\vartheta^2} \right] \left[\frac{a^2}{\gamma \vartheta} - \vartheta \right] + \left[\frac{1}{\vartheta} + \frac{\alpha^2 f a^2}{\gamma \vartheta^3} \right]. \quad (7b)$$

Here, $n = (\gamma - 1)^{-1}$, γ being the polytropic index. At the sonic point, the numerator and the denominator both vanish. From $D = 0$, one obtains the Mach Number $M_c(x_c)$,

$$M_c^2(x_c) = \frac{[\alpha^2 f + n + 1 + \{\alpha^2 f(\alpha^2 f + 1) + (n + 1)^2\}^{1/2}]}{[\gamma(2n + 1)]} \approx \frac{2n}{2n + 1} \quad \text{for } \alpha \ll 1 \quad (8a)$$

For $N = 0$, one obtains an exact expression for the velocity of sound a ,

$$a_c(x_c) = \frac{2\mathcal{A}}{(\mathcal{B}^2 - 4\mathcal{A}\mathcal{C})^{1/2} - \mathcal{B}} \quad (8b)$$

where,

$$\mathcal{A} = \gamma(2n + 1 - \frac{2\alpha^2 f}{\gamma M_c^2}) \left[\frac{1}{2(x-1)^2} - \frac{l_{in}^2}{x^3} \right]$$

$$\mathcal{B} = -\frac{2l_{in}\alpha}{x^2 M_c} (2n + 1 + f - \frac{2\alpha^2 f}{\gamma M_c^2})$$

and

$$\mathcal{C} = -(2n + 2 - \frac{2\alpha^2 f}{\gamma M_c^2}) \frac{5x-3}{2x(x-1)} - \frac{\alpha^2}{\gamma M_c^2 x} (2n + 1 + f - \frac{2\alpha^2 f}{\gamma M_c^2})$$

For $\alpha = 0$, eq. (8a) goes over to $M_c^2(x_c) = 2n/(2n + 1)$ as in C89 and over to $M(x_c) = 1$ for $\gamma = 1$ (isothermal flow) as in C90a. Similar limit is obtained for $a_c(x_c)$ as well. These

conditions allow us to obtain solutions with one *less* parameter, since two extra vanishing conditions of numerator and denominator provide two equations while only one extra unknown (x_c) is introduced. The number of parameters required to study shocks does not change (Abramowicz & Chakrabarti, 1990; C89, C90b). Sonic points occur only where the sound speed is real and positive (Liang & Thomson, 1980; Abramowicz & Zurek, 1981) and the saddle type sonic points (which are vital to a global solution, see C90b) occur when $d\vartheta/dx|_c$ is real and of two different signs (Thompson & Stewart, 1985; Ferrari et al. 1985; C90b). It is easy to see that above constraints can allow a maximum of two saddle type sonic points (vital to a shock formation) when $\gamma \lesssim 1.5$. For higher γ , only inner saddle type sonic point may form, depending on viscosity and accretion rates (responsible for cooling parameter g) unless the flow is of constant height, in which case both sonic points will form even for $\gamma = 5/3$ (MSC96).

In order to study shock waves around a black hole, it is crucial to know if the flow has more than one saddle type sonic point. In a neutron star accretion, one saddle type point is sufficient. This is due to the fundamental difference in the inner boundary conditions. In a black hole accretion, the flow first passes through the outer sonic point, and then, if it passes through a shock, the flow becomes subsonic. It has to pass through another sonic point to satisfy the ‘supersonic’ boundary condition on the horizon with the radial velocity equal to the velocity of light and the rotational velocity locked-in with the rotational velocity of the horizon. At a neutron star boundary, the flow is subsonic, and thus after a shock the flow need not pass through a sonic point. If it does, however, it has to have another shock to satisfy the inner boundary condition and the corotation condition with the star surface. We shall present exact solutions of these kinds in later sections. Not only the flow should have two saddle type points, the entropy at the inner sonic point should be higher compared to the entropy at the outer sonic point and the energy at the inner sonic point must be smaller or equal to the energy at the outer sonic point (C89). For a wind

flow, these considerations are exactly the opposite. Thus, one must know the nature of the energy and entropy densities at the sonic points.

Fig. 1a shows entropy $s(x_c) \propto a(x_c)^{2n}/\rho(x_c)$ vs. specific energy $E(x_c) = 0.5\vartheta^2 + (\gamma - 1)^{-1}a(x_c)^2 + 0.5 l(x_c)^2/x_c^2 - 0.5 (x_c - 1)^{-1}$ plots at the *sonic points* for $\gamma = 4/3$ and $\alpha_P = 0, 0.4, 0.8$. The arrows on the curves in the direction of increasing sonic point location x_c . Two side-by-side curves are for $f = 0$ (cooling dominated) and $f = 1$ (heating dominated) respectively (as marked on the curves). For $\alpha_P = 0$, these two curves coincide. Solid, dashed and dotted regions of the curves are the saddle, nodal and spiral (circle type for $\alpha_P = 0$) type sonic points respectively (C89, C90a,C90b). The branches *AMB* and *CMD* (while referring similar branches of curves with non-zero viscosity and heating parameter f , we shall use same notations such as *AM*, *MB* etc., though we did not mark them on this plot for clarity) are the results on the inner (x_{in}) and the outer (x_{out}) sonic points with *M* being the point where an inviscid flow can pass through the inner and outer sonic points simultaneously. The general “swallow tail singularity” as seen in these figures was noticed by Lu (1985) though importance of having different entropy at different sonic points was not noted as a result it was thought that a flow with the same outer boundary condition may have multiple solutions and bi-periodicities (e.g. Abramowicz & Zurek, 1981; Lu, 1985). Parameters around the point *M* are important to study shock waves in the flow (C89, C90a, C90b). Note that as viscosity is increased, more and more region containing saddle type sonic points become spiral and nodal type, particularly, the outer saddle type sonic point recedes farther and the inner one proceeds inward. For a shock in accretion to be possible, pre-shock flow parameter must lie somewhere on the branch *MD* and the post-shock flow parameter must lie somewhere on *MB* as long as the energy and entropy conditions: $E(x_{in}) \leq E(x_{out})$ and $s(x_{in}) \geq s(x_{out})$ are satisfied. Similarly, for a shock in winds, the pre-shock and post-shock flows must lie on the branches *AM* and *MC* respectively. Typical Rankine-Hugoniot transitions (energy

preserving) are shown by horizontal arrowed dashed lines; difference in entropies at arrow heads determine the entropy generated at the shocks. In the cases where viscosity (heating) or g (cooling) is non-zero, the considerations are the same, except that the transitions are not necessarily horizontal even for Rankine-Hugoniot shocks, because the energy of the flow at the two sonic points could be quite different. A typical such shock transition in the accretion $a \rightarrow a$ is shown on the $\alpha_P = 0.8$ curve (see, C89). For a VTF, the intersection (like M) still separates two basic types of flows. As the viscosity and f is increased, the outer sonic point may no longer remain saddle type and only the inner sonic point may exist. Thus shock transition may no longer be possible. Flow parameters (e.g., the inner sonic point) originally on the branch of type AM , move over to the branch of type MB (i.e., below M) as α_P is increased from 0 to α_{c1} . Thus for $\alpha_P < \alpha_{c1}(x_{in})$, the flow will pass through the inner sonic point and join to a Keplerian disk at a large distance (x_{Kep} is determined by eq. 4a). These flows will stay on the branch AM and can participate in shock-free accretion only and not in accretion shocks. They can also take part in outwardly moving winds. If $\alpha_P > \alpha_{c1}(x_{in})$, the flow with the same x_{in} , will belong to the branch MB and shocks become possible. However, it escapes the shock region for $\alpha_P > \alpha_{c2}(x_{in})$. Thus, for $\alpha_P > \alpha_{c2}$, the flow may pass through the inner sonic point without the shock, although, due to higher viscosity x_{Kep} is smaller (eq. 3a). It is to be noted that the dichotomy in topology in terms of the variation of α as discussed here is valid only when x_{in} and l_{in} are held fixed. When α is held fixed, however, critical angular momentum or critical sonic point location would be obtained which would similarly separate the topologies.

The origin of the critical viscosities is illustrated in Fig. 1b, where we plot two sets of curves, one for $\alpha = 0$ and the other for $\alpha = 0.01$ (marked) around the crossing point M . The curves marked “inner” and “outer” represent the quantities as the inner and the outer sonic points are respectively varied. Heating efficiency factor $f = 0$ is assumed for illustration. A flow which can pass through an inner sonic point marked “A” even without

viscosity (C89) will approach the point “M” (namely, in a zone which can produce shocks in winds) as viscosity is increased. For $\alpha_P = \alpha_{c1}$, the point “A” coincides with “M”. α_{c1} clearly has to depend on the location of “A” itself, namely, the inner sonic point x_{in} through which the flow must pass. The inner sonic point x_{in} , in turn, depends on the specific energy and cooling processes in the flow. With further increase of viscosity, the flow having the same sonic point x_{in} will slide down this region (and reach at “a”, for example, for $\alpha_P = 0.01$) while passing through the zone of accretion-shocks (just below M). The point marked “B”, which was originally within the zone of accretion-shocks, would escape to “b” for $\alpha = 0.01$. This escaping process is the origin of α_{c2} . It is easy to show that increasing the cooling parameter g (or, decreasing heating parameter f) has exactly the opposite effect on the quantities belonging to the inner sonic point. However, the branch representing the outer sonic point acts differently. The flow originally passing through the outer sonic point at “C” slides away (to “c”) from the midpoint “M” as viscosity is increased. This point thus goes out of the region in which wind shocks could form (C89). Similarly, the flow with outer sonic point at “D”, which is capable of participating in an accretion shock (C89) approaches the midpoint “m” and soon cross over “m” so that accretion shocks can no longer form for the flow passing through that particular outer sonic point. The effect of increasing the cooling parameter g (or, reducing the heating parameter f) is also the same. Increasing f brings back the point “d” into accretion shock region, and thereby increasing the critical viscosity parameter for which shocks can form. These important conclusions will be illustrated in the next section.

It is to be noted that the actual values of α_{c1} and α_{c2} themselves are not only functions of the heating and cooling parameters and the location of the sonic points (or, equivalently, energy density of the flow), they also depend on the viscosity prescriptions that is employed. Thus, e.g., critical viscosity parameters for α_P prescription would be roughly twice as much as for α_{Π} prescription. Similarly, it would be a little different if $W_{x\phi}(1)$ stress were

used throughout. The only relevant point is that these two critical values exist which distinguishes flow topologies.

3.2. Π -Stress

In this case, the analysis is carried out with $W_{x\phi} = -\alpha_{\Pi}\Pi$. This is used in computing the angular momentum distribution (3b). Q^+ is computed using MISStress prescription of Section 3.1.

$$\frac{d\vartheta}{dx} = -\frac{N}{D}, \quad (9)$$

where the numerator N is,

$$\begin{aligned} N = & \left[\frac{2n+1}{a} - \frac{4na\alpha_{\Pi}\omega}{(2n+3)\vartheta} \right] \left[a \frac{5x-3}{2x(x-1)} + \frac{\gamma}{a} \left(\frac{l^2}{x^3} - \frac{1}{2(x-1)^2} \right) \right] \\ & + \frac{5x-3}{2x(x-1)} - \omega \left[\alpha_{\Pi}\vartheta \left(\frac{2n}{2n+3} \frac{a^2}{\vartheta^2} + 1 \right) - \frac{2l^2}{x^2} \right] \end{aligned} \quad (10a)$$

and the denominator D is,

$$D = \left[\frac{2n+1}{a} - \frac{4na\alpha_{\Pi}\omega}{(2n+3)\vartheta} \right] \left[-\frac{\gamma}{a} \left(\vartheta - \frac{a^2}{\gamma\vartheta} \right) \right] + \frac{1}{\vartheta} - \alpha_{\Pi}\omega \left(1 - \frac{2n}{2n+3} \frac{a^2}{\vartheta^2} \right). \quad (10b)$$

Here,

$$\omega = \frac{\alpha_{\Pi}f}{\vartheta} \left[\frac{2n}{2n+3} + \frac{\vartheta^2}{a^2} \right].$$

The exact expressions for the Mach number and the sound velocity at the sonic point x_c are given by,

$$\begin{aligned} M_c^2(x_c) = & \frac{n+1 - \alpha_{\Pi}^2 f \frac{2n(4n+5)}{(2n+3)^2} + \left[(n+1)^2 - \frac{8n\alpha_{\Pi}^2 f(n+1)^2}{(2n+3)^2} + \gamma^2 \alpha_{\Pi}^4 f^2 \left(\frac{2n}{2n+3} \right)^4 \right]^{1/2}}{\gamma(2n+1) - \gamma\alpha_{\Pi}^2 f \left(\frac{4n}{2n+3} \right) + \alpha_{\Pi}^2 f} \\ & \approx \frac{2n}{2n+1} \text{ for } \alpha_{\Pi} \ll 1 \end{aligned} \quad (11a)$$

and

$$a_c(x_c) = \frac{-\mathcal{B} + (\mathcal{B}^2 - 4\mathcal{A}\mathcal{C})^{1/2}}{2\mathcal{A}} \quad (11b)$$

where,

$$\begin{aligned} \mathcal{A} &= \mathcal{D} \left[\frac{5x_c - 3}{2x_c(x_c - 1)} + \frac{\gamma\alpha_\Pi^2}{M_c^2 x_c} + \frac{5x_c - 3}{2x_c(x_c - 1)} + \alpha_\Pi^2 f \left(\frac{2n}{2n+3} + M_c^2 \right)^2, \right. \\ \mathcal{B} &= 2\mathcal{D} l_{in} \gamma \alpha_\Pi \frac{\frac{2n}{2n+3} + M_c^2}{x_c^2 M_c} + 2\alpha_\Pi f l_{in} \frac{\frac{2n}{2n+3} + M_c^2}{x_c^2 M_c}, \\ \mathcal{C} &= \mathcal{D} \left[\frac{\gamma l_{in}^2}{x_c^3} - \frac{\gamma}{2(x_c - 1)^2} \right], \end{aligned}$$

and

$$\mathcal{D} = (2n + 1) - \frac{\alpha_\Pi^2 f}{M_c^2} \left(\frac{2n}{2n+3} + M_c^2 \right) \frac{4n}{2n+3}.$$

These results also go over to the inviscid solutions (C89) and isothermal solutions (C90a) in appropriate limits. The nature of the sonic points and the behavior are very similar to what is shown in Figs. 1(a-b). Differences occur in the angular momentum distribution of global solutions since Π -stress preserves angular momentum through shock waves as well.

Note that in both of these cases, the heating parameter f always appears along with the α parameter. This is because of our assumption that the advected flux ($Q^+ - Q^-$) could be written as fQ^+ . This immediately implies that, as if, cooling also disappears if $\alpha = 0$. In general this is not true: cooling can proceed independently of the heating process depending on cooling rates which are functions the optical depth and accretion rates. The transonic inviscid disks with bremsstrahlung cooling alone which has this property is studied in MSC96. In this work global solutions which passes through sonic points and shocks are presented as functions of accretion rates.

Recently, Narayan & Yi (1994) considered a similar set of equations (1a)-(1e) and find global solutions using self-similar procedure in Newtonian potential. The solutions with $f \rightarrow 1$ were termed as ‘advection dominated’. Since this treatment is self-similar, flow does not have any preferred length scale, such as sonic points, or shock waves and

therefore the conclusions derived from this work are likely to be inapplicable or incorrect to describe astrophysics around black hole or neutron stars (Narayan & Yi, 1995ab; Narayan, Yi & Mahadevan, 1995; Narayan, McClintock, J.E. & Yi, 1996; Lasota et al., 1996; Fabian & Rees, 1995). For instance, our Fig.1(a-b) would not simply exist in this self-similar treatment. The VTF close to the horizon ($r \sim 10 - 100x_g$) must fall much faster than a self-similar flow because the gravitational pull is stronger than a Newtonian star, and therefore emission properties of the hard component would be seriously affected, though soft components which are emitted from regions far away from the black hole should be less affected. Secondly, as we shall show, the so-called ‘advection dominated solutions’ do not constitute any new class of solutions (indeed the terminology itself is unfortunate since, as well shall see, the flow is actually always rotation dominated close to the black hole, except, perhaps, just outside the horizon. See, Fig. 7a below). We shall comment on other differences later.

Before we present the global solutions, we wish to make a few comments about the viscosity prescriptions and the usefulness of one over the other. In C90a and C90b, we have used both the cases where, $W_{x\phi}(1) = -\alpha P$ and also where $W_{x\phi}(2) = \eta x d\Omega/dx$ and we found (also see, CM95) the results to be similar ($\eta = \alpha P h(x)/\Omega_{Kep}$ is the coefficient of viscosity). In the above discussions we chose the first prescription since it makes the angular momentum distribution completely algebraical (eqs. 4a, 4b). An important corollary is that, we could now start the integration by supplying the integration constant l_{in} and the inner sonic point x_c only and *derive* the location x_{Kep} from which the flow deviates from Keplerian disk.

On the other hand, if the second prescription of the viscous stress is used, the angular momentum distribution would be (C90a, C90b; CM95),

$$l - l_{in} = \frac{\alpha_P P x^3 h}{\dot{M} \Omega_{Kep}} \frac{d\Omega}{dx}. \quad (12)$$

By virtue of the identification of l_{in} to be the flow angular momentum on the horizon, the flow automatically becomes shear free on the horizon. With this stress, it is easy to show that,

$$\frac{d\vartheta}{dx} = \frac{N}{D}, \quad (13)$$

where, the numerator N is,

$$N = \frac{2n}{2n+1} \frac{5x-3}{2x(x-1)} + \frac{l^2}{a^2 x^3} - \frac{1}{2a^2(x-1)^2} + \frac{f\gamma(l-l_{in})^2\vartheta}{\sqrt{2}\alpha_P a^4 x^{5/2}(x-1)(2n+1)} \quad (14a)$$

and the denominator D is,

$$D = \frac{1}{\vartheta} \left(\frac{\vartheta^2}{a^2} - \frac{2n}{2n+1} \right) \quad (14b)$$

The first term is related to the geometric compression of the flow, second and the third terms represent a competition between the gravity and centrifugal force. The fourth term (containing f is the contribution from the heating/cooling effects. This term comes separately in the numerator exactly as in the case of bremsstrahlung (MSC96) except that in latter case the term appears with an opposite sign consistent with cooling in presence of weak viscosity ($f < 0$). Otherwise the condition $N = 0$ here is not very helpful since it requires a knowledge of $l(x_c)$ which is itself a priori not known (eq. 12). The expression is consistent with $\alpha \rightarrow 0$, $l \rightarrow l_{in}$ or, $x \rightarrow 1$, $l \rightarrow l_{in}$ and thus consistent with inviscid solution of C89 when $f = 0$ is chosen. The denominator gives the Mach number at the sonic point exactly as obtained for inviscid case (C89). One can obtain similar expressions when η in $W_{x\phi}$ is written in terms of the total pressure (ram plus thermal, eq. 7b of CM95).

This prescription, however, poses a few difficulties: (1) one has to solve one extra differential equation (eq. 12) for angular momentum; (2) one no longer has an algebraic condition at the sonic point and therefore study of critical point behavior is difficult (Flammang, 1982), and finally, (3) one definitely has to start the integration from the outer edge x_{Kep} of the flow, particularly when one is using pseudo-Newtonian potential. The problem (3) is severe since it would not be known a priori whether the flow would

go through the sonic point for a given choice of outer boundary condition, or even if it is forced to go, whether the derivatives at the sonic point would be continuous. Because of these reasons, we have chosen the first prescription ($W_{x\phi} = -\alpha_P W$ or $W_{x\phi} = -\alpha_\Pi \Pi$) to consider the angular momentum distribution while adopting MISStress prescription for the cooling term.

If the cooling term were chosen using $W_{x\phi} = -\alpha_P P$ prescription, one would have Q^+ as:

$$Q^+ = \frac{W_{x\phi}^2}{\eta} = \alpha_P P h(x) \Omega_{Kep} \sim \alpha_P P a / \sqrt{\gamma} \quad (15)$$

the sonic point analysis becomes more simplified. The general result, however, remains qualitatively the same.

No matter what prescriptions are used, the positivity of the sound speed at the sonic point (obtained from the vanishing condition $N = 0$) requires that the angular momentum at the sonic point be sub-Keplerian (cf. eq. 8b, 14a). This was pointed out by Abramowicz & Zurek (1981) in the context of adiabatic accretion (see, C90b). We prove in this paper that any transonic disk is necessarily sub-Keplerian at least in some region at and near the sonic point, provided the advective term $Q^+ - Q^- > 0$, *i.e.*, $f \gtrsim 0$. Of course, when the flow is super-cooled ($f < 0$) it *can* be sonic even in a super-Keplerian flow depending on the competition between the geometric heating factor and the cooling factor.

4. SOLUTION TOPOLOGIES

To obtain a complete solution, one must supply the boundary values of energy (or, accretion rate) and angular momentum for a given type of viscosity (α) and cooling parameter (g). This is analogous to Bondi solution where only one parameter, namely, energy density or accretion rate is required. Instead of supplying above mentioned

quantities, we supply here one sonic point location x_c and the angular momentum constant l_{in} (Eq. 3). The equations are integrated from the sonic point inward as in C90a and C90b till they reach the black hole horizon or the neutron star surface. Similarly, they are integrated outward till the Keplerian distribution is achieved. In the case of neutron star accretion, one could supply the outer sonic point instead if the star is big enough to engulf the inner sonic point within its surface. Without any loss of generality, we choose the cooling parameter g (i.e., f for a given α) to be a constant in the analysis below.

Our choice of initial parameters x_c and l_{in} stems from the following considerations: since a black hole accretion is transonic (C90ab), the flow has to pass through ‘A’ sonic point at x_c . Secondly, since we want the flow to originate presumably from a Keplerian disk, it has to carry some angular momentum $l(x_{Kep})$, a part of which would be transported away by viscosity and the other part must enter through the horizon. Exact amount of entry of angular momentum l_{in} is not of much concern (unless one is interested in the spin-up process of a black hole). Thus, l_{in} and $l(x_{Kep})$ are related through eq. (3) and we could have, in principle, supplied x_{Kep} instead. But this is very much uncertain (and is physically unintuitive) as it could vary anywhere from 10 to $10^6 x_g$. On the contrary, the acceptable range of the angular momentum of the accreting solution at the inner edge is very small (from, say, 1.5 to ~ 2 , see, C89, C90ab). Thus, our approach has always been to choose the angular momentum at the inner edge as a free parameter, and then integrate backward to see where the flow deviated from a Keplerian disk (i.e., what angular momentum the flow started with) in order to have l_{in} on the horizon. In other words, in our approach, x_{Kep} is the eigen value of the problem. As in C90a and C90b, in what follows, we shall use this approach as well.

4.1. General Behavior of Globally Complete Solutions

Figs. 2(a-b) show examples of global solutions passing through the inner sonic points. In each small box in Fig. 2a, we plot Mach number $M = v/a$ (vertical scale goes from 0 to 2) as function of the logarithmic radial distance (scale goes from 0 to 50). On the upper axis, we write α_{II} parameters (marked as 0.0001, 0.05, 0.2 and 0.4) and on the left axis we write the heating parameter f (marked as 0.0, 0.1, 0.5, and 1.0). Each of the grid number of the 4×4 matrix that is formed is written in the upper-left corner of each box. In Fig. 2b, we show the ratio R (vertical scale goes from 0 to 1.5) of disk angular momentum to the Keplerian angular momentum to emphasize on the degree at which the flow is non-Keplerian. The short-dashed horizontal lines in each box is drawn at $R = 1$. Other parameters fixed for the figures are $x_c = 2.795$, $l_{in} = 1.65$ and $\gamma = 4/3$. In these figures, the sonic points are not located at $M = 1$ but at an appropriate number computed assuming corresponding polytropic index, the viscosity and heating parameter as given in eq. (11a).

Whereas in all these figures the sonic point is saddle type, whether or not the flow will participate in a shock or remain shock-free will depend on its global topology. In the first column of Fig. 2a, the flow is almost inviscid and the results are almost independent of the heating parameter f . The flow joins with the Keplerian disk at several thousand Schwarzschild radii (outside the range of Fig. 2b, but see, Fig. 7b below). The flow leaves the Keplerian disk and enters the black hole straight away through the inner sonic point. This open topology is the characteristics of the parameters chosen from the branch AM of Fig. 1a, i.e., the inflow can pass through inner sonic point without a shock, or, an outflow will form (with or without a shock), depending on where on the branch AM the parameter is located. In the second column, the viscosity is higher, and the topologies are closed. This implies that $\alpha_{\text{II}} > \alpha_{c1}$ is already reached and the same inner sonic point brought the flow from the branch AM to MB . The angular momentum of the flow cannot join a Keplerian disk unless a shock is formed, or the flow is shock free, but passes only through the outer sonic point if it exists. For lower heating parameter the flow topology opens up again

when viscosity parameter is further increased (column 3) and the flow again joins with the Keplerian disk, but only at a tens of Schwarzschild radii (Fig. 2b). In this case, $\alpha_{\Pi} > \alpha_{c2}$ is achieved and the flow topology leaves the accretion shock regime on the branch AM . For a higher heating parameter f , α_{c2} is higher, if the sonic point still remains of saddle type. This is consistent with our understanding (Fig. 1b) that increasing f (or, reducing g) brings back the flow into the shock regime for a given viscosity parameter. Note that as f crosses, say, 0.5, i.e., as the cooling become more inefficient, the integral curves change their character: the spiral with an open end goes from clock-wise to anti-clockwise. The implication is profound. For $f \lesssim 0.5$ the closed spiral surrounding the open spiral can still open up to join a Keplerian disk (e.g., grids 13, 23), but for $f \gtrsim 0.5$ closed spiral can no longer join with a disk (e.g., grids 34,43, they could, in principle open up to a ‘Keplerian wind’!, see also C90a,b). Thus we prove that only for higher cooling ($f \lesssim 0.5$) and higher viscosity ($\alpha > \alpha_{c2}$), Keplerian disk can extend much closer to the black hole, otherwise it must stay much farther away and the transonic advective solution will prevail.

The change of topologies by a change of viscosity is not surprising. Increase in viscosity increases angular momentum at the sonic points. At smaller viscosities, the sub-Keplerian flow becomes Keplerian very far away and as we discussed before (above eq. 3), all the three sonic points could be present. At a high enough viscosity, flow becomes Keplerian very quickly and only one (the inner) sonic point is possible. (Note that we mean the distance from the *horizon* when we use the phrase ‘far away’ or ‘quickly’.)

Though we shall discuss in detail in section §6, we like to point out the important result that the flow with a lower viscosity and higher cooling joins with the Keplerian disk at a farther distance than the flow with a higher viscosity. This implies that a disk with a differential viscosity with lower viscosity at higher elevation can simultaneously have a Keplerian disk on the equatorial plane and a sub-Keplerian disk away from the equator.

This has already been observed in isothermal disks (C90b, CM95) and this consideration has allowed us to construct the accretion disk of more general type (C94, C96a). This also allowed us to obtain the most satisfactory explanation, to date, of the observed transition of soft and high states of galactic black hole candidates (CT95, Ebisawa et al, 1996). A similar picture of accretion flow is obtained when α is kept fixed (even increasing vertically upward) for the entire disk, but l_{in} or x_{in} also increases away from the equatorial plane. One requires very special cooling efficiencies to fulfill these constraints.

We continue to emphasize the importance of the understanding of the nature of the inner sonic points, by varying its locations as in Fig. 3a. We mark x_{in} in each box and keep other parameters fixed: $\gamma = 4/3$, $\alpha_{\Pi} = 0.05$, and $f = 0.5$. As the sonic point location is increased, the open topology of the flow (in branch AM) becomes closed (in branch MB) and ultimately the physical solution ceases to exist as the inner sonic point no longer remained saddle type (cf. Fig. 1a). The only available solutions remain those passing through the outer sonic point (discussed later). Note that the inner sonic point continues to remain saddle type even when it crosses $r = 3x_g$, i.e., marginally stable orbit. This is because the marginally stable orbit in fluid dynamics (i.e., in presence of pressure gradient forces) does not play as much special role as in a particle dynamics. It is easy to show that the similar crossing at $r = 3x_g$ takes place for a large range of α parameters. In Fig. 3b, we vary angular momentum l_{in} (marked on the upper axis) and the heating parameter f (marked on the left axis) while keeping $x_{in} = 2.8$ and $\alpha_{\Pi} = 0.05$. We note that for very low angular momentum, the flow behaves like a Bondi flow, with only a single sonic point. As angular momentum is increased the topology becomes closed and the flow can enter the black hole only through a shock or through the outer sonic point if it exists.

So far, we discussed the nature of the inner sonic point. However, as in an inviscid polytropic flow (Liang & Thomson, 1980; C89), or, isothermal VTF (C90a, and C90b), the

general case that is discussed here also has the three sonic points as is obvious in Fig. 1a. In Fig. 4, we show Mach number *vs.* logarithmic distance when $x_{out} = 35$ is chosen (with the same scale and other parameters as in Fig. 2a). In the first column, with low viscosity, the flow either passes through the outer sonic point only, or can pass through a shock and subsequently through the inner sonic point (if the shock conditions are satisfied). As the viscosity is increased, the topology is closed and the flow parameters must be different so as to allow the flow through an outer sonic point ($x_{out} > 35$) which has an open topology and which smoothly joins with the Keplerian disk farther away. It could also subsequently pass through the inner sonic point if shock conditions are satisfied. The choice must finally depend upon the the flow parameters as illustrated in Fig. 1a. Note that, in general, it is difficult to have a saddle type outer sonic points for higher α_{Π} , partly because it is defined to be about half of α_P and partly because the outer sonic point itself recedes at viscosity is increased (Fig. 1a) and therefore flow does not pass through a given outer sonic point if the viscosity is raised.

4.2. Solutions which Contain Shock Waves

In Fig. 5a, we present Mach number variation with the logarithmic radial distance. The Rankine-Hugoniot conditions (namely, conservation of the mass flux, momentum flux and energy flux at the shock front) in the vertical averaged flow (C89) were used to obtain the shock locations. The flow parameters chosen are $x_{out} = 50$, $l_{in} = 1.6$, $\alpha_{\Pi} = 0.05$, $\gamma = 4/3$ and $f = 0.5$. The shock conditions in turn force the flow to have a shock at $x_{s3} = 13.9$ (using notation of C89) and to pass through the inner sonic point at $x_{in} = 2.8695$. This location is computed by equating its entropy with the amount of entropy generated at the shock and subsequently advected by the flow plus the entropy generated in the post-shock subsonic flow (similar to C90a,b where energy advection conditions were considered).

The shock itself (shown here as the vertical transition with a single arrow) is assumed to be thin and non-dissipative, i.e., energy conserving. In presence of viscosity, the shock would be expected to smear out. Thus x_{s3} calculated assuming infinitesimal shock width represents an ‘average’ distance of the shock from the black hole. We have shown also a double-arrowed vertical transition where a shock will form in a neutron star accretion with subsonic inner boundary condition and the flow locking in with the surface. It is easy to verify that the shock conditions are satisfied at $x = 2.39$. A neutron star of mass $1.4M_{\odot}$ and radius $r_* = 10$ km (i.e, $r_* = 2.38r_g$) will marginally fit within the shock. In case the star surface is bigger than the inner sonic point, the post(single-arrowed)shock branch will be completely subsonic, and not transonic as is shown here. We have also drawn only x_{s3} . The other location $x_{s2} \sim 4$, closer to the inner sonic point is unstable as will be shown below.

In order to show that the shock transitions shown in the above Figure are real, and stable, we show in Fig. 5b, not only the Mach numbers of the subsonic and supersonic branches, but also other physical quantities along these branches. The solid curves represent the branch passing through the outer sonic point located at $x_{out} = x_c = 50$ and the long dashed curves represent the branch passing through the inner sonic point at $x_{in} = x_c = 2.8695$. The flow chooses this subsonic branch for $x < x_{s3}$ since the entropy of the flow is higher at the inner sonic point (C89). We have plotted the shock invariant (C89) function appropriate for a vertically averaged flow,

$$C = \frac{\left[M(3\gamma - 1) + \frac{2}{M}\right]^2}{2 + (\gamma - 1)M^2}, \quad (16)$$

the angular momentum distribution $l(x)$ ($\times 2$), the Mach number distribution $M(x)$, the total pressure Π (in arbitrary units), the local specific energy $E(x)$, radial velocity and the proton temperature $T = \mu m_p a^2 / \gamma k$ (in units of 2×10^{11} K). Here, $\mu = 0.5$ for pure hydrogen, m_p and k are proton mass and Boltzmann constant respectively. At the shock, the temperature goes up and the velocity goes down, in the same way as in our earlier

studies. The solid and dashed curves describing C , Π , $E(x)$ variations intersect at the shock $x = x_{s3} = 13.9$, consistent with the Rankine-Hugoniot condition. Though the total pressure Π in these two branches intersect at two locations suggesting two shocks (as in C89, C90ab) only the one we marked is stable, as can be easily verified by a perturbation of the shock location (CM93). At $x = x_{s3} = 13.9$, if the shock is perturbed outwards, the pressure along the pre-shock flow (solid curve) is higher than that along the post-shock flow (dashed curve) (Fig. 5b). Thus the shock is pushed inwards. Similarly, if the shock is perturbed inwards, it is pushed outwards due to higher pressure in post-shock flow. This is not true for the intersection at $x_{s2} \sim 4$ and therefore the shock solution at x_{s2} is unstable. The location of the shock on the neutron star accretion is also obtained in the same way, but this time one has to compare quantities of the super-sonic branch passing through the outer sonic point, with the quantities of the sub-sonic branch at $x < x_{in}$ (Fig. 5a).

We discussed only about those shock transitions which do not instantaneously release energy or entropy at the shock locations. If they do, the shock conditions have to be changed accordingly (Abramowicz & Chakrabarti, 1990; C90b) and the shock locations appropriately computed.

So far, we chose only $f = \text{constant}$ solutions. One can always choose a suitable function $f(\alpha, x, \dot{M})$ which satisfies $f \rightarrow 0$ for $x \gtrsim x_{Kep}$ and $f \rightarrow 0.5 - 1$ (depending on cooling efficiency) for $x \sim x_c$ and redo our exercise. This will clearly be the combination of results presented above where outer sonic point is chosen for $f = 0$ and inner sonic point is chosen for $f \sim 0.5 - 1$. A cooling function $g(\tau)$ to accomplish this is already presented in Chakrabarti & Titarchuk (1995). Work with actual heating and cooling is in progress, and we shall report them in future.

The difference in the boundary conditions in black hole and neutron star cases give rise to an important observational effect. The bulk motion of the optically thick converging

inflow (Blandford & Payne, 1981) could ‘Comptonize’ soft photons through Doppler effect to produce a hard spectra of slope ~ 1.5 (Chakrabarti & Titarchuk, 1995) observed in the galactic black hole candidates (e.g., Sunyaev et al., 1994). In a neutron star accretion the flow is subsonic close to the surface and such a power law is neither expected nor observed.

In Fig. 6, we present a montage of solutions involving the shock waves for $\gamma = 4/3$. (α_{II}, f) parameter pair is written in each box. Mach number is from 0 to 2 and the radial distance is varied from 0 to 100. The outer sonic points are located at $x_{out} = 50$, and the inner sonic points were determined from the evolution of the flow after the shock, are also shown. In the boxes containing only the flow from outer sonic point, shock conditions were not found to be satisfied in a black hole accretion. We therefore did not draw the branch with inner sonic point, since it would be meaningless to do so. The shocks in black hole and neutron stars for (α_{II}, f) parameters $(0.07, 0.1)$, $(0.05, 0.3)$, and $(0.05, 0.5)$ are located at 15.025 and 2.38, 10.35 and 2.34, and 13.9 and 2.392 respectively. It is to be noted that the self-similar solutions in Newtonian potential (e.g., Narayan & Yi, 1994) shocks cannot form since no length scale is respected by self-similarity assumption and the flow always has constant Mach number and does not pass through sonic points of any kind. It is to be noted that for accretion around a neutron star, two shocks (of type x_{s1} and x_{s3} in C89 notation) may form if the star is compact enough. This would make computation of a neutron star spectra more complicated.

4.3. Advection vs. Rotation, Keplerian vs. Non-Keplerian

As in the past, we define the flow to be advection dominated when $\vartheta > v_\phi = l/x$ and rotation dominated when $\vartheta < v_\phi = l/x$. It is interesting to study whether the flow is dominated by the advection or rotation, as the flow starts deviating from the Keplerian

disk. In Fig. 7a, we present the ratio ϑ/v_ϕ of a few solutions already presented. The solutions with labels ‘11’, ‘12’ and ‘13’ are from the first row and the solution with label ‘43’ is from the third column of Fig. 2a. The solution labeled ‘shock’ corresponds to the case presented in Fig. 5a. Except those marked ‘12’ and ‘43’, other solutions smoothly match with the Keplerian disk at the outer edge as they become more and more rotation dominated. Advection domination starts much closer to the black hole, although, interestingly, flow again becomes rotation dominated as it comes closer to the black hole. At the shock, the flow goes from advection dominated to rotation dominated although the angular velocity itself is continuous (Fig. 7b). The solutions marked ‘12’ and ‘43’ are either to be joined by shock waves (i.e. a flow first passing through the outer sonic point) or, are not possible at all, since they do not by themselves smoothly join with a Keplerian disk.

In Fig. 7b, we present the ratio of disk angular momentum to the local Keplerian angular momentum as a function of the logarithmic radial distance. The curves are labeled by viscosity parameters α_Π . Other parameters of the group labeled ‘A’ are: $l_{in} = 1.88$, $x_{in} = 2.2$, $\gamma = 4/3$, $f = 0$ and of the group labeled ‘B’ are $l_{in} = 1.6$, $x_{in} = 2.8695$, $\gamma = 4/3$, $f = 0.5$. Note that for a given set of flow parameters, as the viscosity is reduced, the location x_{Kep} where the flow becomes Keplerian is also increased (eq. 4a; C90a,b). Secondly, the flow can become super-Keplerian close to a black hole, a feature assumed originally in modeling thick accretion disks (e.g. Paczyński & Wiita, 1980). Thirdly, if the viscosity is high, the flow may become Keplerian immediately close to the black hole. This behavior may be responsible for hard state to soft state transitions in black hole candidates as well as novae outbursts which are known to depend on viscosity on the flow. We discuss this in the final section. Note that the angular momentum distribution of the curve marked 0.05 is continuous even though it has a shock wave at $x_{s3} = 13.9$ (Fig. 5a-b).

Since the thick accretion disks are traditionally considered to be those which are

sub-Keplerian and at the same time rotationally dominated, we find from Figure 7b that there are essentially *two* thick accretion disks, one *inside* the other, so to speak. One is a ‘big’ thick disk, whose outer edge starts where the flow deviates from Keplerian, and the other is a ‘small’ thick disk, which occupies the post-shock flow. Our thick disks are more accurate than traditional thick disks, because we include advection as well.

4.4. Dependence on Polytopic Index

So far, we have discussed the solution topologies, with the polytropic index $\gamma = 4/3$. In general, the index could be higher or lower, depending on the radiation and magnetic field content, and for a fully self-consistent solution one is required to compute this index as the flow evolves, rather than choosing it a constant. This is beyond the scope of the present analysis. In C90a and C90b, we considered $\gamma = 1$ results which would be used for both optically thick or thin advective flows. We now give some flavor of solution topologies when the extreme case of $\gamma = 5/3$ is chosen.

Fig. 8 shows the energy-entropy plot for $\gamma = 5/3$ and $l_{in} = 1.65$. This is to be compared with Fig. 1a, where $\gamma = 4/3$ was used instead. Other notations are identical. The arrow indicates the variation as the sonic point is increased. The important point to note is that, in this case, the outer saddle type sonic point does not exist. In other words, the flow must adjust itself to pass through the inner sonic point alone (shown by the solid curves). A corollary of this is that the flow will not have a centrifugally supported shock wave, as discussed here, unless the flow is already supersonic at the outer boundary (or, the flow geometry is different, e.g., MSC96) or the shock is not centrifugally supported but forms due to some other effects (such as, external heating; see, e.g. Chang & Ostriker, 1985). It is easy to show that similar absence of the outer sonic point prevails for $\gamma \geq 1.5$ (see, Fig.

3.1 of C90b). It is possible that relativistic flows close to a black hole has $\gamma \sim 13/9$ (e.g., Shapiro & Teukolsky, 1983), thus may be the possibility of shocks are more generic.

Finally, for the sake of completeness, we close this section by showing the behavior of the solution topologies for $\gamma = 5/3$. In Fig. 9a, we vary viscosity and heating parameters as in Fig. 2a. Other parameters are: $x_{in} = 2.8$, $l_{in} = 1.65$. With these choices, the topology is closed even for an inviscid flow. As the viscosity is increased, the topology opens up and joins with a Keplerian flow. If we started with an initially open topology, similar to $\gamma = 4/3$ case, we would have two critical viscosities causing similar topological changes as in Fig. 1a. In Fig. 9b, we show the topologies when heating parameter f and the angular momentum l_{in} (marked on the left axis) and the location of the inner sonic point x_{in} (marked on the upper axis) are varied.

5. ON THE COMPLETENESS OF THE GLOBAL SOLUTIONS

Using simple combinatorics, we briefly argue here that there could be no other topologically distinct VTF solution other than what we described in this paper. For a physical solution, the final sonic point through which the flow must pass (either outer or inner) just before entering a black hole should be of saddle type. Let us denote them by S_+ (positive slope) and S_- (negative slope) solutions respectively. In the inviscid case, central sonic point is center type or ‘O’ type (say, O for convenience) which splits into two spiral type solutions which may be clockwise or anti-clockwise when viscosity, heating and cooling are added. Let us denote them by P_+ for clockwise spirals and P_- for anti-clockwise spirals. Clearly, the following combinations of these sonic points (from inner edge outwards) form an exhaustive set: S_+S_- , $S_+S_-OS_+S_-$, $S_+(S_-P_-)(P_-S_-)S_+$, $(S_+P_+)(S_-P_-)S_+S_-$, $S_-(S_+P_+)(P_+S_+)S_-$, $S_+S_-(P_+S_+)(P_-S_-)$. These handful of choices

are dictated by the fact that a saddle type solution with a positive slope can only join with a clockwise spiral (this ‘joining’ is indicated by parenthesis) and a saddle type solution with a negative slope can only join with an anti-clockwise spiral. Except the second case with ‘O’ type point, which we found in the inviscid flow (C89), the rest have been shown in various figures of the previous section and C90a and C90b. Although we consider only vertically averaged flow here, the topologies are not expected to change when a ‘thick’ quasi-spherical flow is considered. Indeed, the presence of shocks would be more generic as they would appear even outside the equatorial plane because of weaker gravity. Similarly, when a Kerr black hole is used, the centrifugal barrier become stronger with the increase of the Kerr parameter because the horizon gets smaller. Thus, the shocks are formed for much wider parameter range in Kerr geometry.

A fundamental assumption which allowed us to simply classify these solutions is that the radial forces involved in the momentum equation (eq. 1a) are ‘simple enough’ so that the velocity variation of the flow could still be reduced into the form (6) or (9) since both the numerator and the denominator are only *algebraic* functions and do not involve differential operators. In the present context, this was possible by choosing $W_{x\phi} = -\alpha P$ prescription of shear stress. Even then, if the force were more complicated, as in the case of cooler wind solutions from mass losing stars where radiative acceleration term with nonlinear dependence of velocity gradient is included (Castor, Abbott & Klein, 1975), it would not be possible to reduce the governing equations into a first order differential equation (vital to the discussions of Bondi-type solutions). Critical curves, instead of critical points would be present (Flammang, 1982; C90b) solution topologies of which would be more complex. Discussion on this is beyond the scope of the present analysis.

6. DISCUSSION AND CONCLUSIONS

In this paper, we presented for the first time the global solutions of transonic equations in presence of viscosity, advection, rotation, *generalized* heating and cooling. Our VTF solution starts from a Keplerian disk at the outer edge and enters through the horizon after passing through sonic point(s). As in our earlier studies of inviscid (C89) and isothermal VTFs (C90a and C90b), we emphasized here the possibility of the formation of the shock as well where two transonic solutions are joined together by means of Rankine-Hugoniot conditions. Though we have used general considerations of heating and cooling, we note that no new topologies of solutions emerge other than what are discussed in C90a and C90b. However, unlike in C90a and C90b, where critical viscosities are studied only in the context of shock formation, our detailed study here indicates that there are indeed two types of critical viscosities both of which depend on the parameters of the flow. For $\alpha < \alpha_{c1}$, accretion through inner sonic point is only allowed (i.e., no shock) or winds with or without shock is allowed. In this case, the flow joins with a Keplerian disk very far away (Fig. 2a). For $\alpha_{c1} < \alpha < \alpha_{c2}$ the flow can have shocks if shock conditions are satisfied, else the flow will pass through the outer sonic point. For $\alpha > \alpha_{c2}$, the flow will pass through inner sonic point again. In this case, the flow joins a Keplerian disk very close ($x \sim 10x_g$) to the horizon. Whether both of these critical viscosity parameters exist will depend on the flow parameters, such as the location of one sonic point, the angular momentum at the inner edge l_{in} and the heating parameter f . Once we specify these quantities, the entire solution topology, including the shock location (if present), and the location where the flow joins with a Keplerian disk are completely determined. Our results depend on the accretion rate through the cooling parameter g (or, equivalently, through f) and always produce stable branch of the solution in the $\dot{M} - \Sigma$ plane. This is possibly because of our choice that the cooling could be written as a constant fraction of heating term. We also show that when the polytropic index is higher than 1.5, in a vertically averaged flow model the outer sonic point does not exist (though it exists if the disk is thinner, see, MSC96), and therefore,

shocks are possible only if the flow at the outer boundary is already supersonic. Since the total pressure Π (and not the thermal pressure) is continuous across the shock waves, we used the Π -stress prescription (CM95) to study shock waves. This prescription is always valid, and we recommend its uses for the study of astrophysical flows around black holes and neutron stars, where the advection effect, and therefore ram pressure is important.

Since our VTF solutions have one *less* free parameter, the $\dot{M}(\Sigma)$ relation is monotonic with positive slope and always represents the stable solutions. In other words, the thermal/viscous instability is removed completely by the addition of advection effects. This is true whether or not the flow contains a shock wave. When more general cooling law is used (with power law dependence on accretion rates, for example), it is possible that our stable solutions could be ‘destabilized’ in some parameter space spanning \dot{M}, Σ as originally discussed by Meyer & Meyer-Hofmeister (1983) (see also, Cannizzo, 1993). Thus, the problem with our model is not ‘how to stabilize the inner edge of a Keplerian disk’ but rather, ‘how to destabilize the perfectly stable transonic disks’, if indeed, the novae outbursts are signatures of such instability. Similarly, because of our choice of cooling law $Q^- \propto Q^+$, we are unable to show direct influence of accretion rate onto to the cooling efficiency. Our parametrization indicates that for *any* accretion rate, higher or lower efficiency of cooling is possible, just by changing the viscosity parameter. Furthermore, we find that the variation of x_{Kep} with α could be achievable by varying x_{in} and l_{in} as well (Fig. 3) even when the entire flow has constant viscosity parameter α . These questions are easily answered by assuming exact cooling laws as far as possible. We shall examine these solutions in near future.

Unlike the properties of the more complex VTF models, where non-linear radiative accelerations play major roles, we used simpler momentum equation, relevant for hot flows close to a compact object. This enabled us not only to obtain global solutions in general,

but also to discuss about the complete set of topologies. Indeed, the same topologies were seen in isothermal VTFs (C90a and C90b), and we argued that no other type of solutions are possible either. The same conclusion holds even when more general cooling laws (such as with power law dependence on density and temperatures) are employed (MSC96). Our results have the same accuracy as that of the description of the pseudo-Newtonian potential of a Schwarzschild geometry. But as we discussed in the introduction, no new topologies have been discovered for inviscid flows when full general relativistic models are solved (C96b). However, under some circumstances the torque can become negative and the angular momentum is transported inward. This happens just outside the horizon and does not affect the solution topologies.

Having not discovered any new topologies, we believe that the unified scheme of global solutions presented by us (C93, C94, C95, CM95) with the knowledge of isothermal disks remains valid even for disks with general heating and cooling. In C94, we wrote “... These findings are very significant as they propose a unifying view of the accretion disks. This incorporates two extreme disk models into a single framework: for inviscid disks, strong shocks are produced, and for disks with high enough viscosity, the stable shock disappears altogether and angular momentum can become Keplerian.” Our present grand unified global solution describes the most general form of accretion which goes over to the other disk models presented in the literature. This is not surprising, since we exactly solve the most general equations. Our disk can pass through either or both the sonic points (when shocks are present) while joining smoothly with the Keplerian disk at a distance x_{Kep} . The post-shock flow, where the disk is rotationally dominated (Fig. 7a) behaves exactly as the thick accretion disks (e.g. Paczyński & Wiita, 1980; see MLC94). If the shock does not form, the sub-Keplerian optically thin flow will behave similar to the ion-supported tori (Rees et al. 1982) because cooling is inefficient in an optically thin flow, and the entire energy remains conserved and is advected away (C89). However, our solution is more consistent

than a conventional thick disk model as we include advection term as well, and obtain the global solutions (see also related discussions in CT95). In MLC94, we have already verified that the results of vertically averaged solution (C89) are sufficiently accurate. Our solutions indicate that winds may be produced from the inflow with positive energy (C89; Fig. 1a) which are verified through extensive numerical simulations (MLC94, Ryu et al. 1995). A knowledge of the dependence of x_{Kep} on viscosity enabled us to construct the most general form of accretion disk, in which Keplerian disk in the equatorial plane is flanked by sub-Keplerian flows above and below. Post-shock hot matter Comptonizes soft-photons from the Keplerian disk to produce hard X-rays (CT95). This understanding has resolved the long standing problem of transition of states of black hole spectra. Furthermore, MSC96 shows that shock oscillations could be responsible for the quasi-periodic oscillation. The difference of the inner boundary condition in the neutron star and black holes has resulted in a difference in spectral index from the emergent spectra in soft states (CT95). Our most general solution can also provide explanations of more complex phenomena, such as the spectral evolution observed during novae outbursts (Ebisawa et al., 1996). For instance, during the quiescence stage, viscosity being low, the disk deviates from being Keplerian farther away (Figs. 2a, 7a, 7b) and the generally optical radiation is accompanied by very weak X-rays which are produced due to reprocessing of the soft radiation intercepted by the sub-Keplerian inner disk. As the viscosity at the outer edge is increased due to piling up of matter (e.g., Cannizzo, 1993), the sub-Keplerian flow first rushes in close to the black hole (since the in fall time scale is shorter for a sub-Keplerian flow) increasing the hard X-ray component as commonly observed in the pre-outburst phases (Ebisawa et al., 1994). Subsequent increase in Keplerian matter close to the black hole increases soft-X-ray component as is observed. Thus, the present *grand unification* of the accretion solutions is more complete, and successfully bridges the gap between the well studied spherical Bondi flow (e.g., Shapiro, 1973a,b; Ostriker et al., 1976; Begelman, 1978; Colpi, Maraschi &

Treves, 1984; Wandel, Yahil & Milgrom, 1984; Blondin, 1986; Begelman & Chiueh, 1988; Park & Ostriker, 1989; Park 1990; Nobili, Turolla & Zampieri 1991) and the Keplerian disks of Shakura & Sunyaev (1973) and Novikov & Thorne (1973). An important ramification of having sub-Keplerian disks is that the azimuthal velocities are less than that of a Keplerian flow. The masses of the central object determined from such considerations (e.g., using Doppler shifts of emitted lines) are naturally higher (Chakrabarti, 1995) than what it would have been if Keplerian motions were assumed instead. Similarly, due to inefficiency of emission processes in disks with advection, the masses of the central black holes in active galaxies (which traditionally equates central luminosities with Eddington luminosities) might have been seriously underestimated (C96). Fabian & Rees (1995) raise such concerns recently using self-similar, super-advective flow solutions. However, since we found that the angular momentum in the accretion is no less than 20 – 50 percent of the Keplerian disk, the conclusions would be expected to be less dramatic.

The author acknowledges the hospitality of Max-Planck Institute (Garching) and Landessternwarte (Heidelberg) in the summer of 1994, where this work was partially completed. He thanks R. Khanna and Stefan Appl (both at Landessternwarte) for discussions. He also thanks an unknown referee and Paul Wiita for the encouragement to expand a smaller, cryptic version of this work originally submitted to *Astrophysical Journal Letters* (also in the e-print archive under astro-ph/9508060). The present research is supported through a Senior Research Associateship award from National Academy of Sciences.

REFERENCES

- Abramowicz, M.A. & Chakrabarti, M.A. 1990, ApJ, 350, 281
- Abramowicz, M.A., Czerny, B., Lasota, J.P. & Szuzkiewicz, E. 1988, ApJ, 332
- Abramowicz, M.A. & Zurek, W.H. 1981, ApJ, 246, 314
- Anderson, M.R., & Lemos, J.P.S. 1986, MNRAS, 233, 489
- Begelman, M.C. & Chiueh, T. 1988, ApJ, 332, 872
- Begelman, M.C. 1978, MNRAS, 185, 847
- Blandford, R.D. & Payne, D.G. 1981, MNRAS, 194, 1033
- Blondin, J.M. 1986, ApJ, 308, 755
- Cannizzo, J.K. 1993, in *Accretion Disks in Compact Stellar Systems*, ed. J. Craig Wheeler (Singapore: World Scientific).
- Castor, J.I., Abbott, D.C., & Klein, R.I. 1975, ApJ, 195, 157.
- Chakrabarti, S.K. 1985, ApJ, 288, 1 (C85)
- Chakrabarti, S.K., Jin, L., & Arnett, W.D. 1987, ApJ, 313, 674
- Chakrabarti, S.K. 1989, ApJ, 347, 365 (C89)
- Chakrabarti, S.K. 1990a, MNRAS, 243, 610 (C90a)
- Chakrabarti, S.K. 1990b, *Theory of Transonic Astrophysical Flows* (Singapore: World Scientific) (C90b)
- Chakrabarti, S.K. 1990c, ApJ, 362, 406
- Chakrabarti, S.K. 1990d, ApJ, 350, 275
- Chakrabarti, S.K. 1990e, MNRAS, 246, 134
- Chakrabarti, S.K. 1992, MNRAS, 256, 300

- Chakrabarti, S.K. in Numerical Simulations in Astrophysics, Eds. J. Franco, S. Lizano, L. Aguilar & E. Daltabuit (Cambridge University Press: Cambridge, 1993) [C93]
- Chakrabarti, S.K. 1994, in Proceedings of 17th Texas Symposium (New York Academy of Sciences, New York) [C94]
- Chakrabarti, S.K. 1995, ApJ, 441, 576 [C95]
- Chakrabarti, S.K. 1996a, Physics Reports, 266, No. 5-6, 238 [C96a]
- Chakrabarti, S.K. 1996b, MNRAS, in press [C96b]
- Chakrabarti, S.K., & Molteni, D. 1993, ApJ, 417, 671 [CM93]
- Chakrabarti, S.K., & Molteni, D. 1995, MNRAS, 272, 80 [CM95]
- Chakrabarti, S.K., & Titarchuk, L. 1995, ApJ (Dec 20th) [CT95]
- Chang K. M., & Ostriker, J. P. 1985, ApJ, 288, 428
- Colpi, M., Maraschi, L. & Treves, A. 1984, ApJ, 280, 319
- Ebisawa, K. et al. 1994, PASJ, 46, 375
- Ebisawa, K., Titarchuk, L.G., & Chakrabarti, S.K. 1996, PASJ, 48, No.1 in press
- Englmaier, P. Diploma Thesis, University of Heidelberg (1993).
- Fabian, A.C., & Rees, M.J. 1995, MNRAS, in press
- Flammang, R.A. 1982, MNRAS, 199,833
- Ferrari, A., Trussoni, E., Rosner, R. & Tsinganos, T. 1985, ApJ, 294, 397
- Frank, J., King, A.R., & Raine, D.J., Accretion Power in Astrophysics (Cambridge University Press, Cambridge, 1991)
- Ipsier, J.R. & Price, R.H. 1982, ApJ, 255, 654
- Lasota, J.P., Abramowicz, M., Chen, X., Krolik, J.H., Narayan,R., & Yi, I. 1996, preprint

- Liang, E.P.T & Thomson, K.A., 1980, ApJ, 240, 271
- Lu, J.F., 1985, A&A, 148, 176
- Matsumoto, R., Kato, S., Fukue, J., & Okazaki, A.T. 1984, PASJ, 36, 71
- Mészáros, P. 1975, A & A, 44, 59
- Meyer, F., & Meyer-Hofmeister, E. 1983, A&A, 128, 420
- Molteni, D., Lanzafame, G., & Chakrabarti, S.K. 1994, ApJ, 425, 161 [MLC94]
- Molteni, D., Sponholz, H., & Chakrabarti, S.K. 1996, ApJ (in press) [MSC96]
- Muchotrzeb B. 1983, Acta Astron., 33, 79
- Nakayama, K. 1982, MNRAS, 259, 259
- Narayan, R., 1996, in “Basic Physics of Accretion Disks” eds. S. Kato et al., Gordon and Breach Science Publishers (New York, 1996) in press
- Narayan, R., & Yi, I. 1994, ApJ, 428, L13
- Narayan, R., & Yi, I. 1995a, ApJ, 444, 231
- Narayan, R., & Yi, I. 1995b, ApJ, in press
- Narayan, R., Yi, I., & Mahadevan, R. 1995, Nature, 374, 623
- Narayan, R., McLintock, J.E., & Yi, I. 1996, ApJ, in press
- Nobili, L., Turolla, R. & Zampieri, L. 1991, ApJ, 383, 250
- Nobuta, K. & Hanawa, T. 1994, PASJ, 46, 257
- Novikov, I. & Thorne, K.S. in: Black Holes, eds. C. DeWitt and B. DeWitt (Gordon and Breach, New York, 1973).
- Ostriker, J.P., McCray, R., Weaver, R. & Yahil, A. 1976, ApJ, 208, L61
- Paczynski, B. & Bisnovatyi-Kogan, G. 1981, Acta Astron., 31, 283

- Paczynski, B. & Wiita, P.J. 1980 *A&A*, 88, 23
- Park, M.G., 1990, *ApJ*, 354, 64
- Park, M.G., & Ostriker, J.P. 1989, *ApJ*, 347, 679
- Pringle, J. 1981, *Ann. Rev. Astron. Astrophys.*, 19, 137
- Rees, M., M. J., Begelman, M. C., Blandford, R. D., & Phinney, E. S. 1982, *Nature*, 295, 17
- Ryu, J., Brown, G., Ostriker, J. & Loeb, A. 1995, *ApJ*, (in press).
- Shakura, N.I. & Sunyaev, R.A. 1973, *A&A*, 24, 337 [SS73]
- Shapiro, S.L. 1973a, *ApJ*, 180, 531
- Shapiro, S.L. 1973b, *ApJ*, 1185, 69
- Shapiro, S.L. & Teukolsky, S.A., *Black Holes, White Dwarfs and Neutron Stars — the Physics of Compact Objects* (John Wiley & Sons, New York, 1983)
- Sunyaev, R. A. et al., 1994, *Astron. Lett.* 20, 777
- Spruit, H.C. 1987, *A & A*, 184, 173
- Taam, R.E. & Fryxell, B.A., 1985, *ApJ*, 294, 303
- Takahashi, M., Nitta, M., Tatematsu, Y., Tomimatsu, A. 1990, *ApJ*, 363, 206
- Tanaka, Y. in *Proceedings of the 23rd ESLAB symposium*, ed. J. Hunt & B. Battrick, vol. 1, p.3, 1989, (ESA, Paris)
- Thompson, J.M.T. & Stewart, H.B., *Nonlinear Dynamics and Chaos* (John Wiley & Sons Ltd., 1985)
- Wandel, A., Yahil, A. & Milgrom, M., 1984, *ApJ*, 282, 53

Fig. 1(a-b): Variation of specific entropy as functions of specific energy $E(x_c)$ at sonic points. Location of the sonic point increases along the direction of the arrow on the curves. Solid, long-dashed and short-dashed curves represent saddle type, nodal type, and spiral type sonic points respectively. Three groups of curves are drawn for the viscosity parameter $\alpha_P = 0.0, 0.4$ and 0.8 (as marked) and two side by side curves in each group are for cooling and heating dominated (marked) cases (for $\alpha_P = 0$ these two curves coincide). $l_{in} = 1.65$ and $\gamma = 4/3$ are chosen. The branches of the type marked AMB correspond to the inner sonic points, and branches of the type marked CMD correspond to outer sonic points. Horizontal arrows mark typical Rankine-Hugoniot shock transitions in winds (upper) and accretion (lower) respectively. In (b), the region near M is zoomed to illustrate the origin of critical viscosities. Sonic points slide along the curves as the viscosity and the cooling parameters are changed. See text for details.

Fig. 2(a-b): Variation of Mach number with logarithmic radial distance as viscosity parameter α_{II} (marked on the upper axis) and the heating parameter f (marked on the left axis) are varied. Inner sonic point $x_{in} = 2.795$ and angular momentum constant $l_{in} = 1.65$ are chosen. Note the changes in topologies and α_{II} crosses the critical viscosities. In (b), the ratio R of disk and Keplerian angular momenta are shown, the horizontal short-dashed lines mark $R = 1$. For low and high viscosities the flow joins Keplerian disk, but for intermediate cases the disk must have a shock or pass only through the outer sonic point to join a Keplerian disk and the horizon.

Fig. 3(a-b): Same as Fig. 2a, but (a) location of sonic point x_{in} (marked in each box), and (b) angular momentum l_{in} (marked on the upper axis) and heating parameter f (marked on the axis on left) are varied.

Fig. 4: Same as Fig. 2a, but the outer sonic point is held fixed at $x_{out} = 35$ while varying the viscosity and heating parameters.

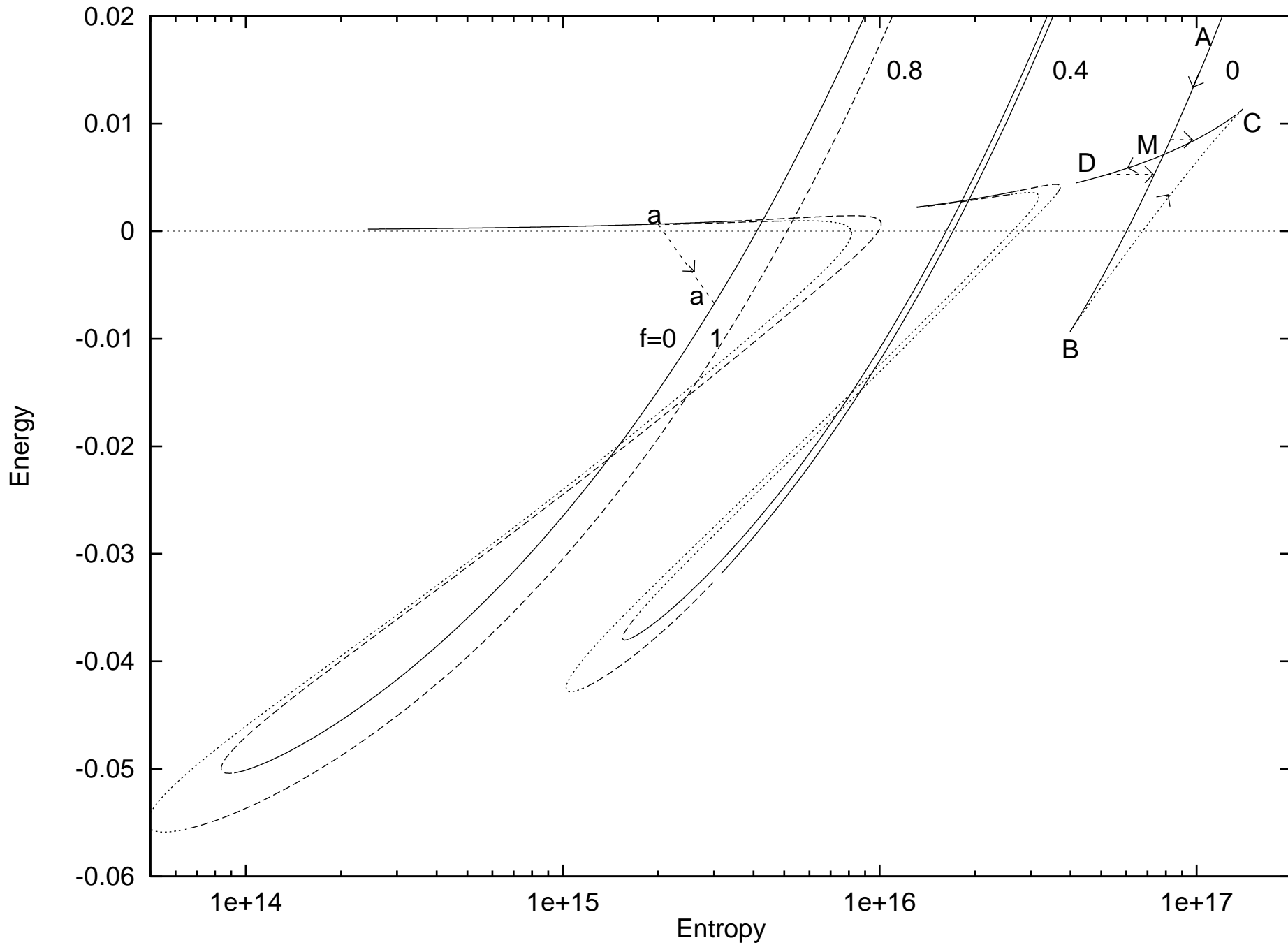
Fig. 5(a-b): Example of a complete solution which includes a shock wave. $\alpha_{\text{II}} = 0.05$, $l_{\text{in}} = 1.6$, $\gamma = 4/3$ and $f = 0.5$, $x_{\text{out}} = 50$ are used. Shock conditions are satisfied at $x = 13.9$ (vertical dashed curve) and the flow subsequently enters the black hole along the long dashed curves after becoming supersonic at $x_{\text{in}} = 2.8695$. The arrowed curves trace the complete solution with a shock wave in a black hole accretion. Double arrowed curves denote the shock solution in a neutron star accretion with sub-sonic inner boundary condition. In (b), the procedure of obtaining the shock solutions is illustrated by plotting the Mach invariant C , the total pressure Π and the energy $E(x)$ of the subsonic and super branches all of which intersect at the shock location. Note that the angular momentum remains continuous across the shock. Other physical quantities, such as the proton temperature and the radial velocity are also shown.

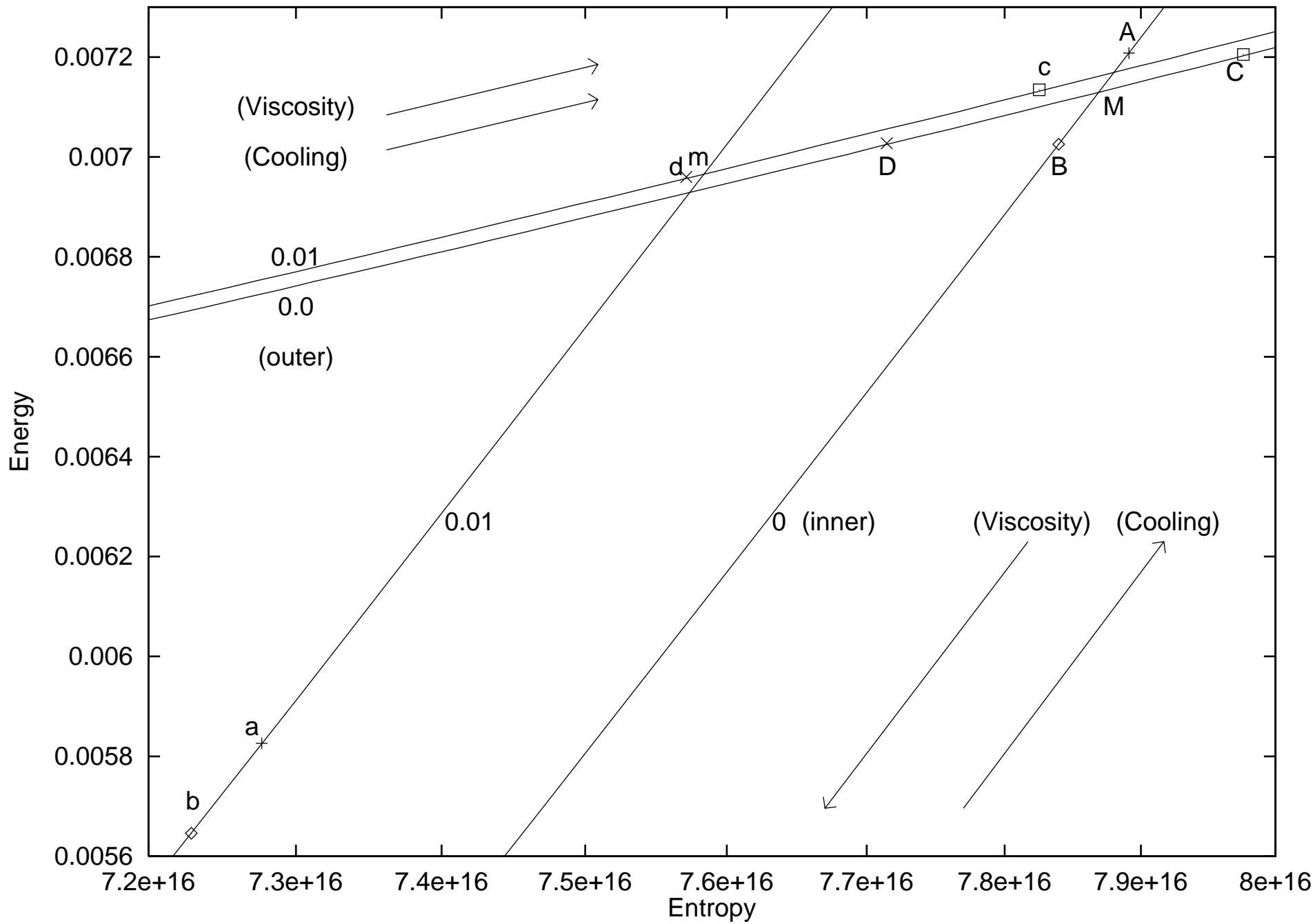
Fig. 6: Parametric dependence on the formation and location of shocks in black hole and neutron star accretions. Single arrows represent shocks in accretion around black holes while the double arrows represent shocks around compact neutron stars. Pairs of parameters (α_{II}, f) are shown in each box. The outer sonic point is chosen to be at $x_{\text{out}} = 50$. In the neutron star case, the shock transition takes place only to that particular sub-sonic branch which corrotates with the star at the star surface.

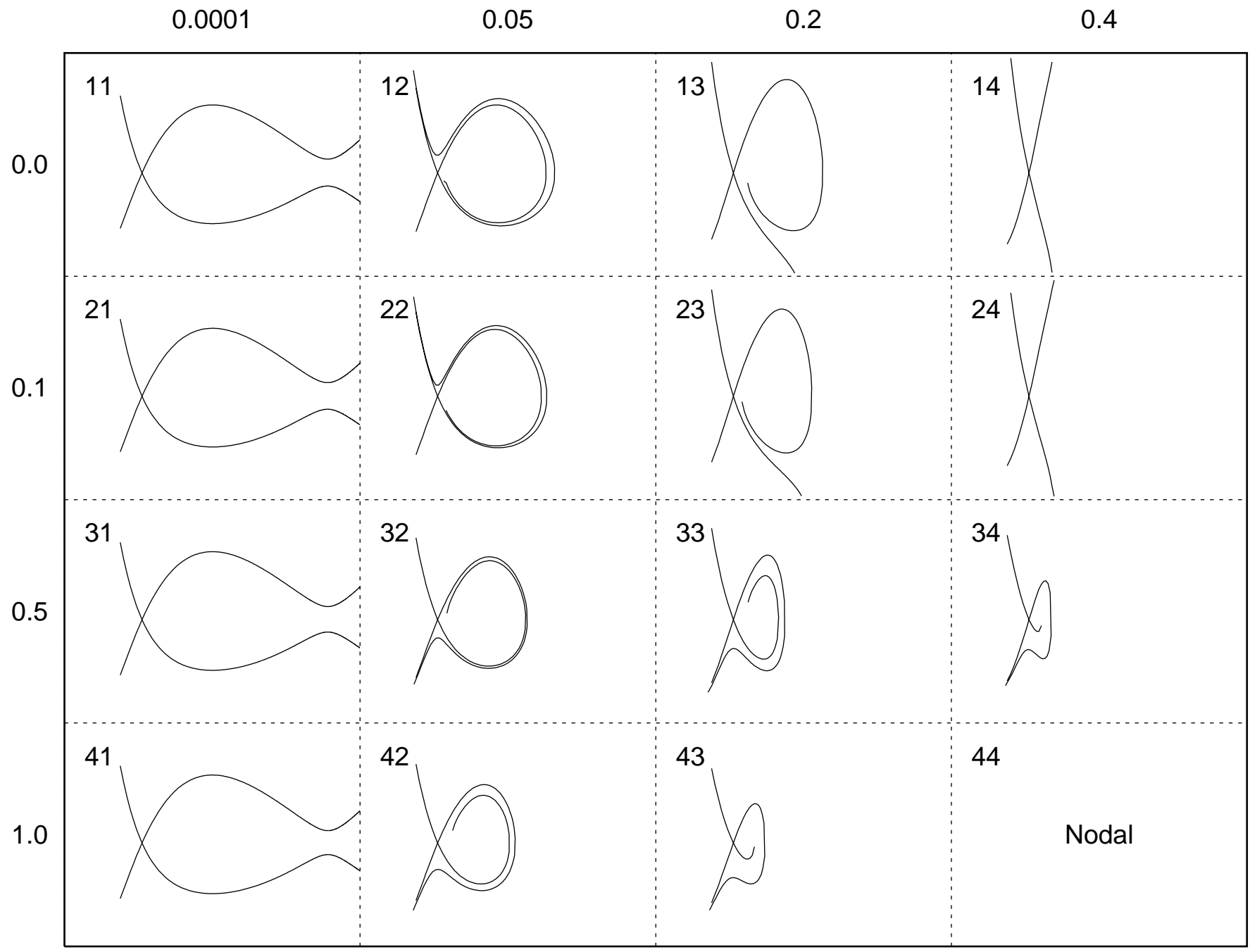
Fig. 7(a-b): Ratio of (a) radial to azimuthal velocities (v_r/v_ϕ) and (b) disk angular momentum to Keplerian angular momentum (l/l_{Kep}) are shown in a few solutions. In (a) the curves marked with numbers correspond to the grid number of Fig. 2a. The curve marked ‘shock’ correspond to the solution in Fig. 5a. Solutions except those marked ‘43’ and ‘12’ join smoothly with Keplerian disks as they become rotation dominated. In (b), the curves are marked with viscosity parameters (the curve marked 0.05 correspond to the shock solution in Fig. 5a). Note that x_{Kep} , where the flow joins a Keplerian disk, depends inversely on the viscosity parameter. See text for detail.

Fig. 8: Same as Fig. 1a, but drawn for $\gamma = 5/3$ to illustrate that the outer saddle type sonic point does not exist (a feature shared by flows with $\gamma > 1.5$ in a vertically averaged model). Thus the flow from a Keplerian disk must pass only through the inner sonic point. Centrifugally supported shocks could form only if the flow at outer boundary is already supersonic (e.g., originated from stellar winds).

Fig. 9(a-b): Similar to Figs. 2-3, showing the variation of solution topologies when $\gamma = 5/3$ is chosen. See text for details.





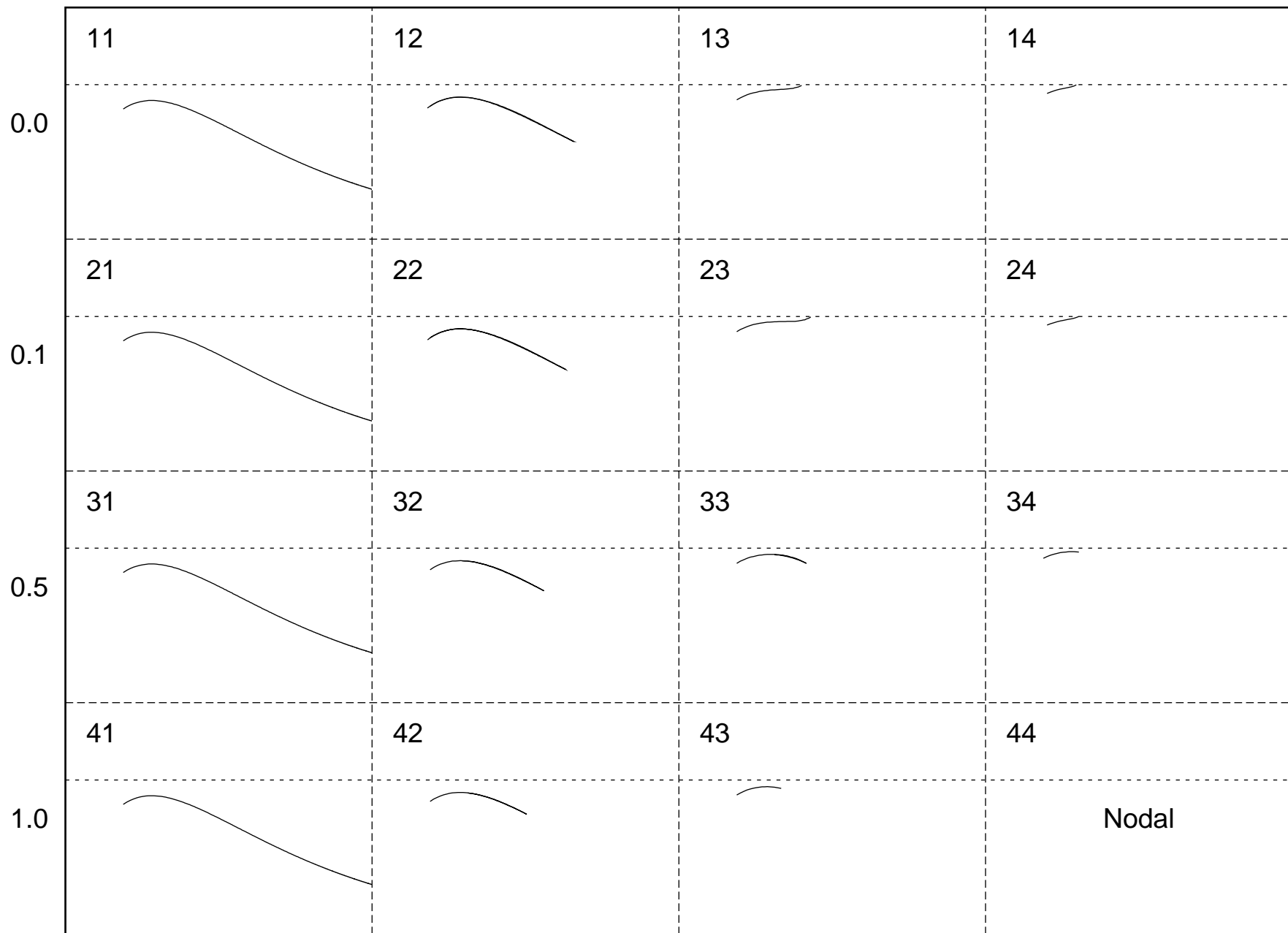



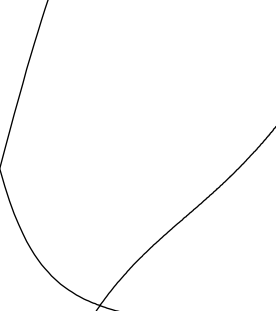


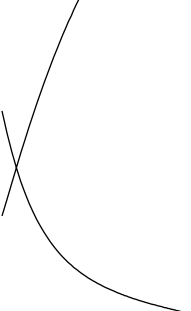
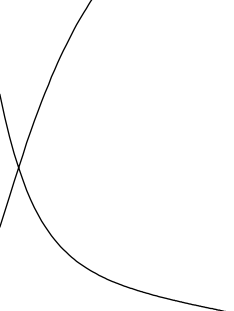
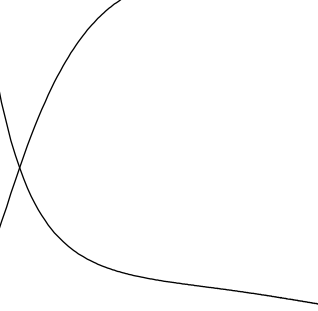
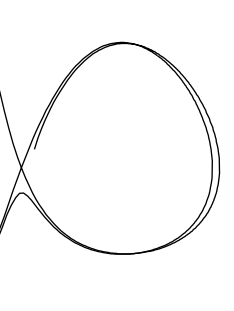
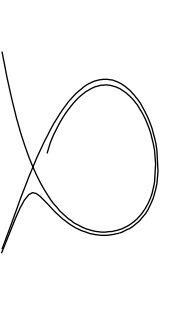
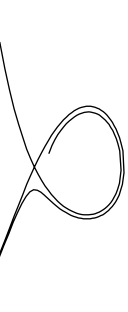




0.0001

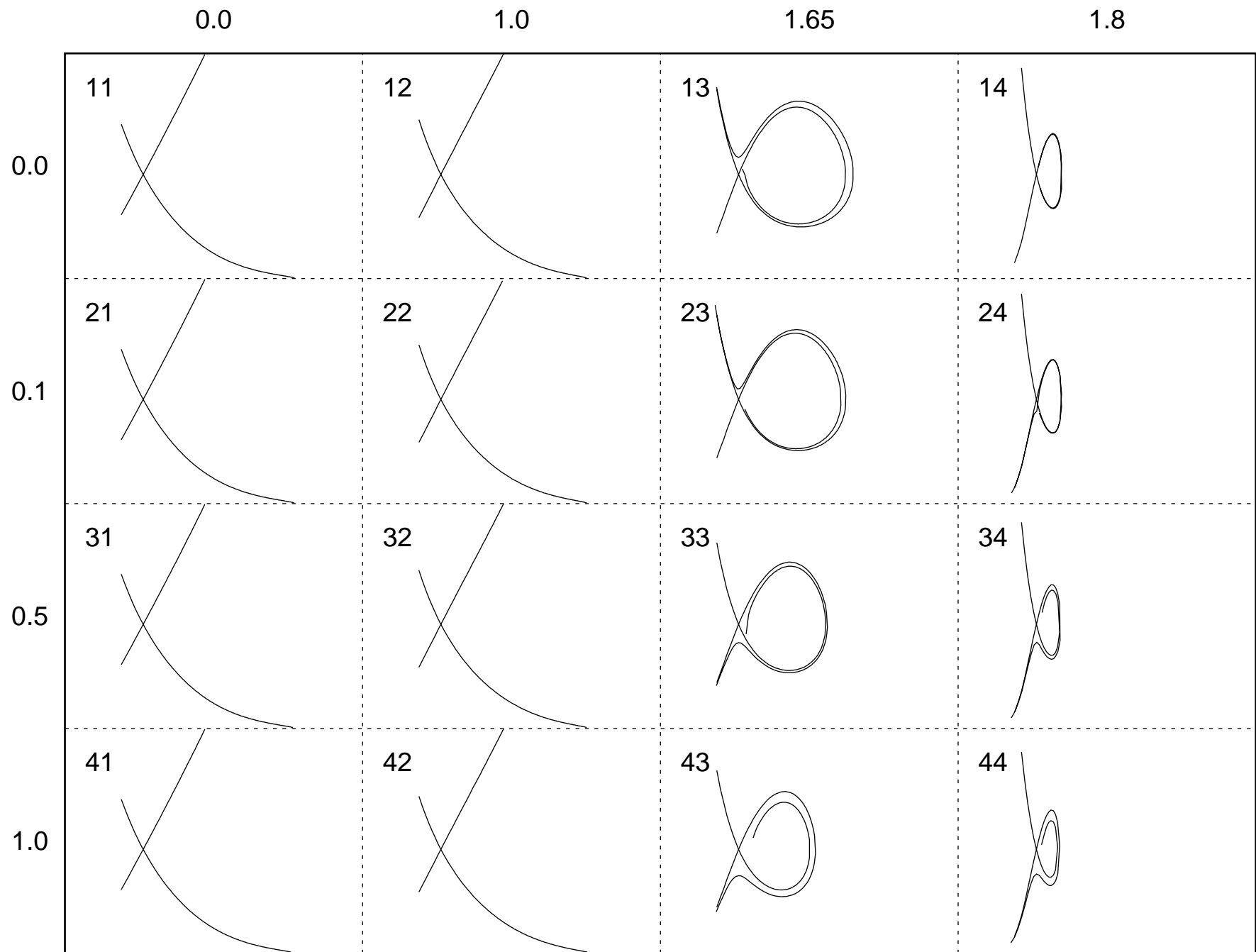
0.05

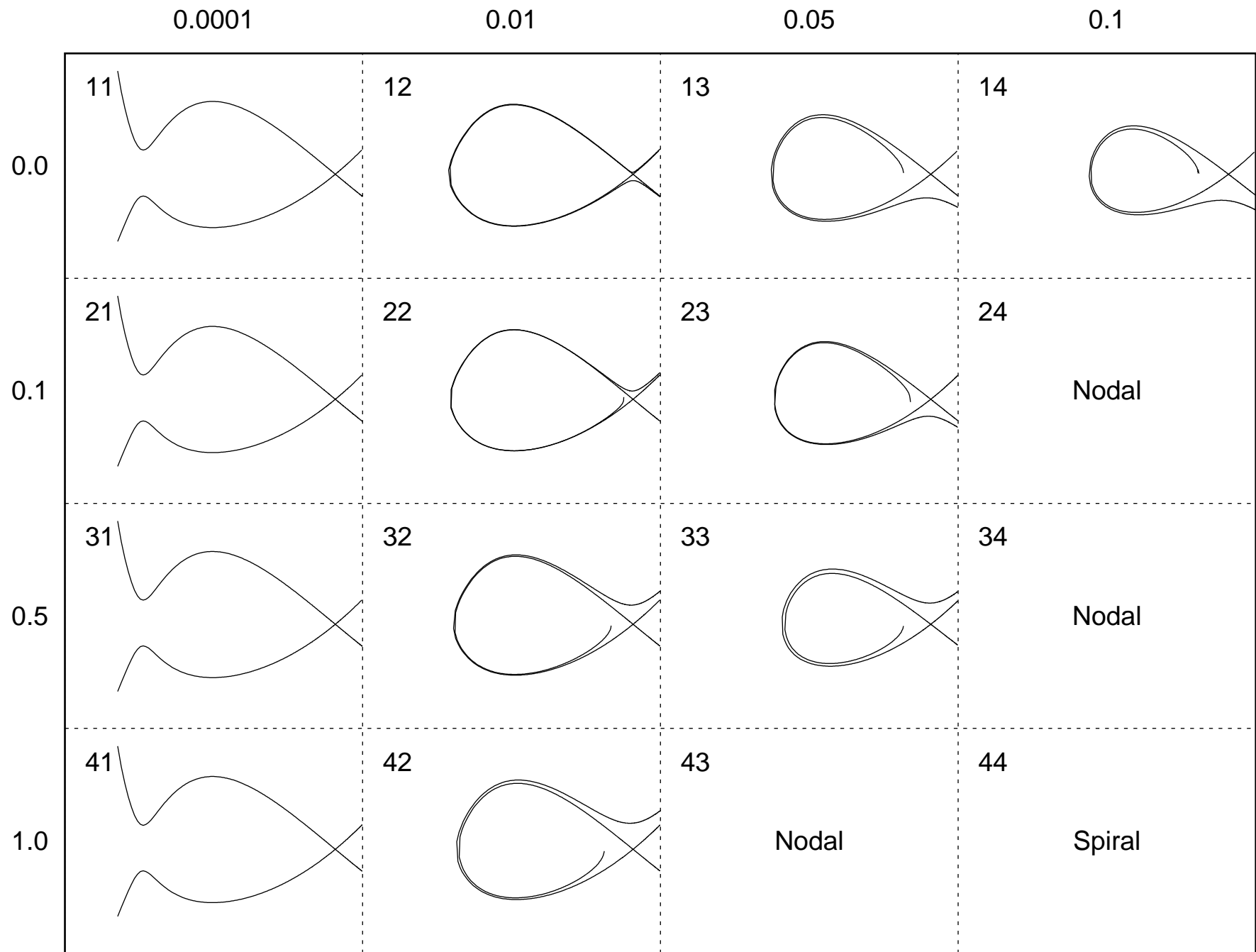
0.2

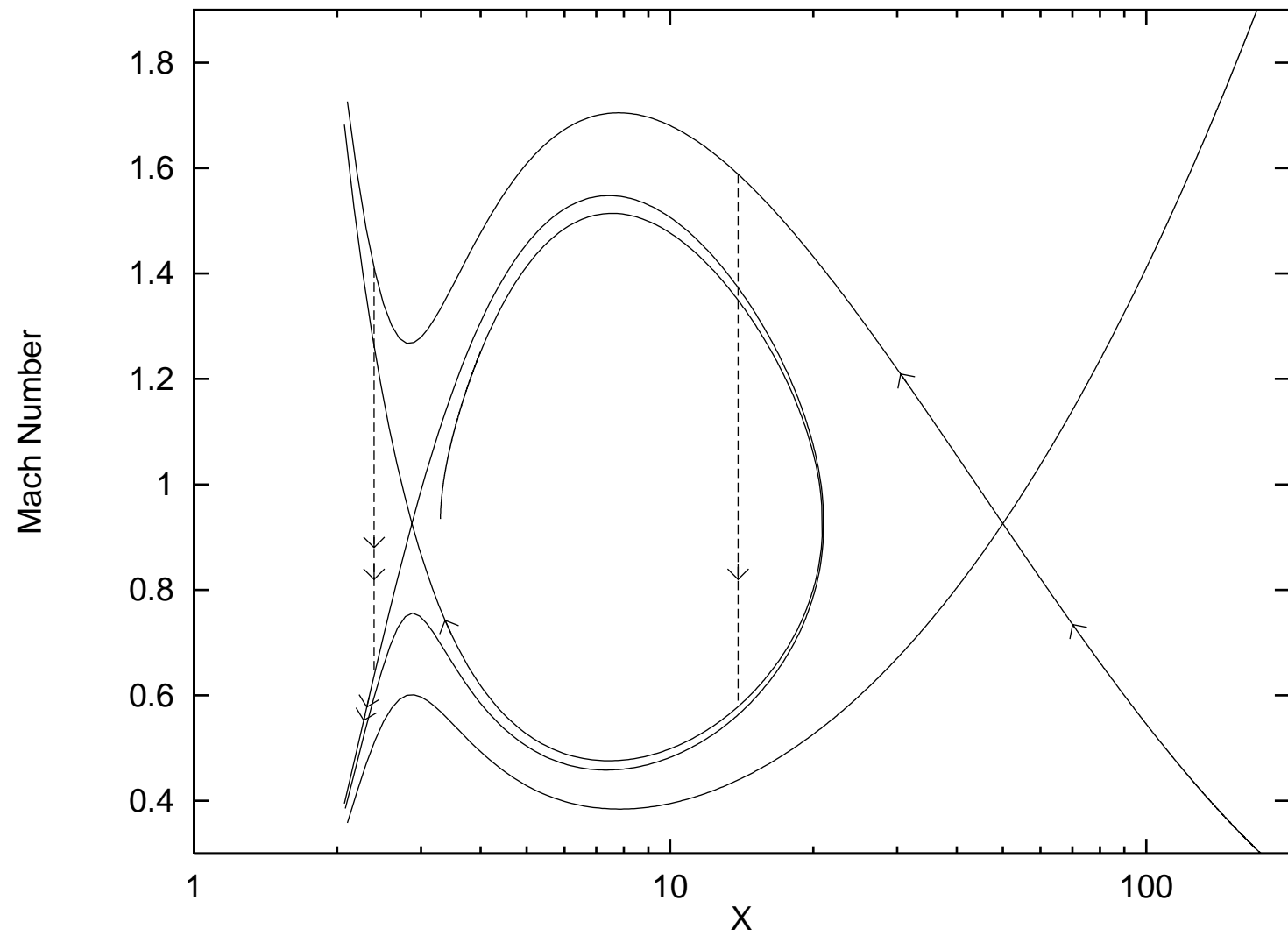
0.4

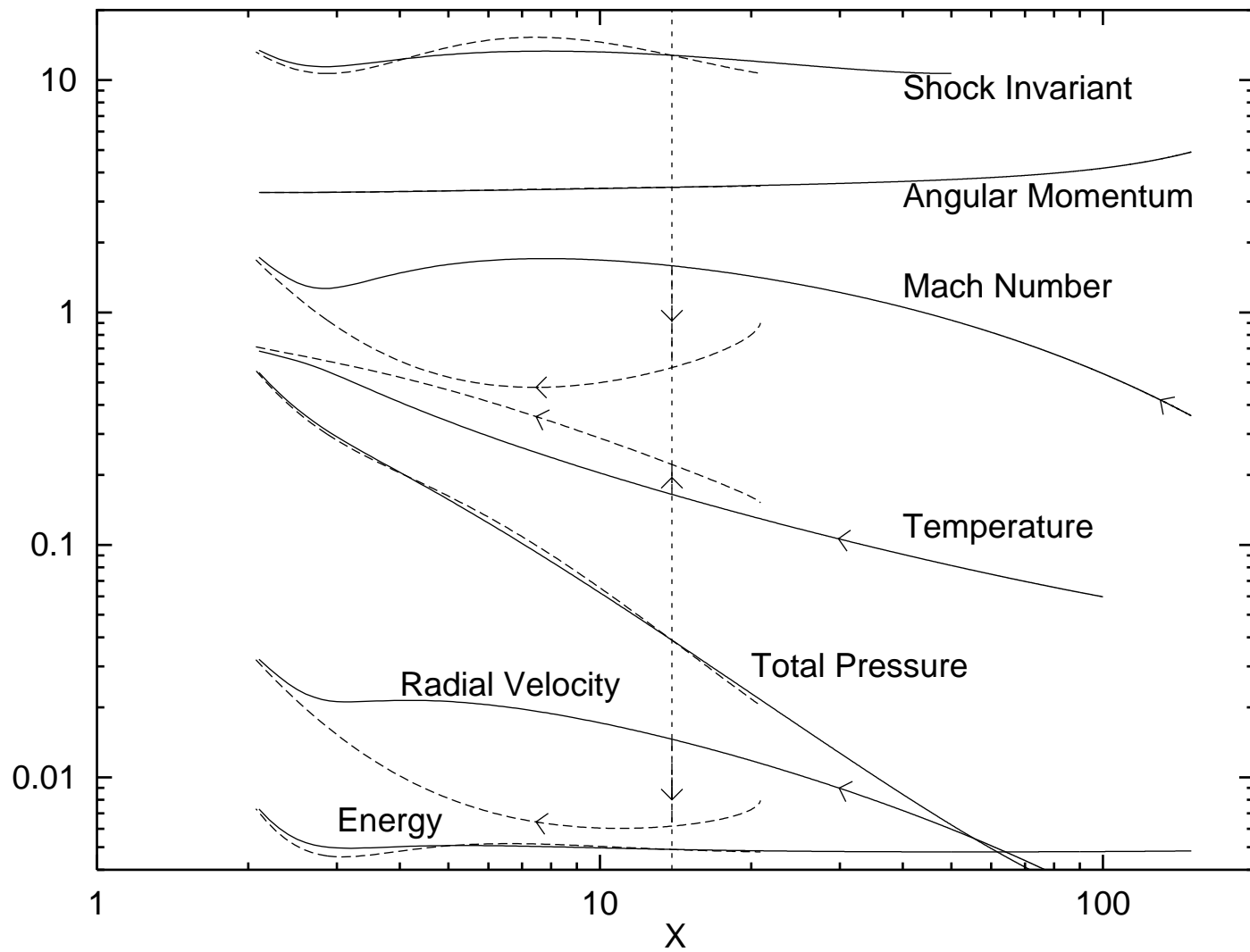


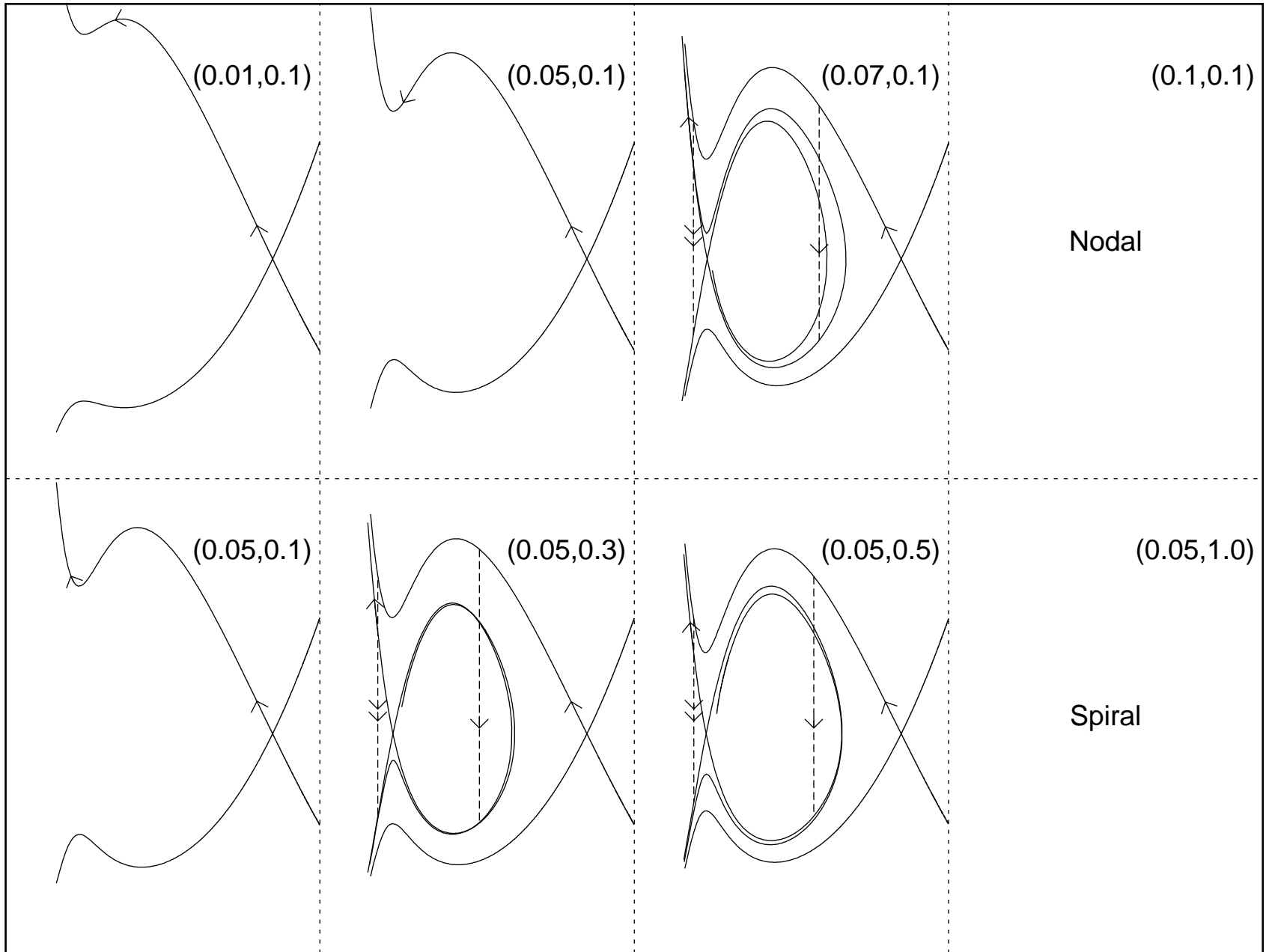
<p>2.05</p> 	<p>2.1</p> 	<p>2.2</p> 	<p>2.3</p> 
<p>2.4</p> 	<p>2.5</p> 	<p>2.6</p> 	<p>2.7</p> 
<p>2.8</p> 	<p>2.9</p> 	<p>3.0</p> 	<p>3.1</p> 
<p>3.2</p> 	<p>3.3</p> 	<p>3.4</p> <p>Spiral</p>	<p>3.5</p> <p>Spiral</p>



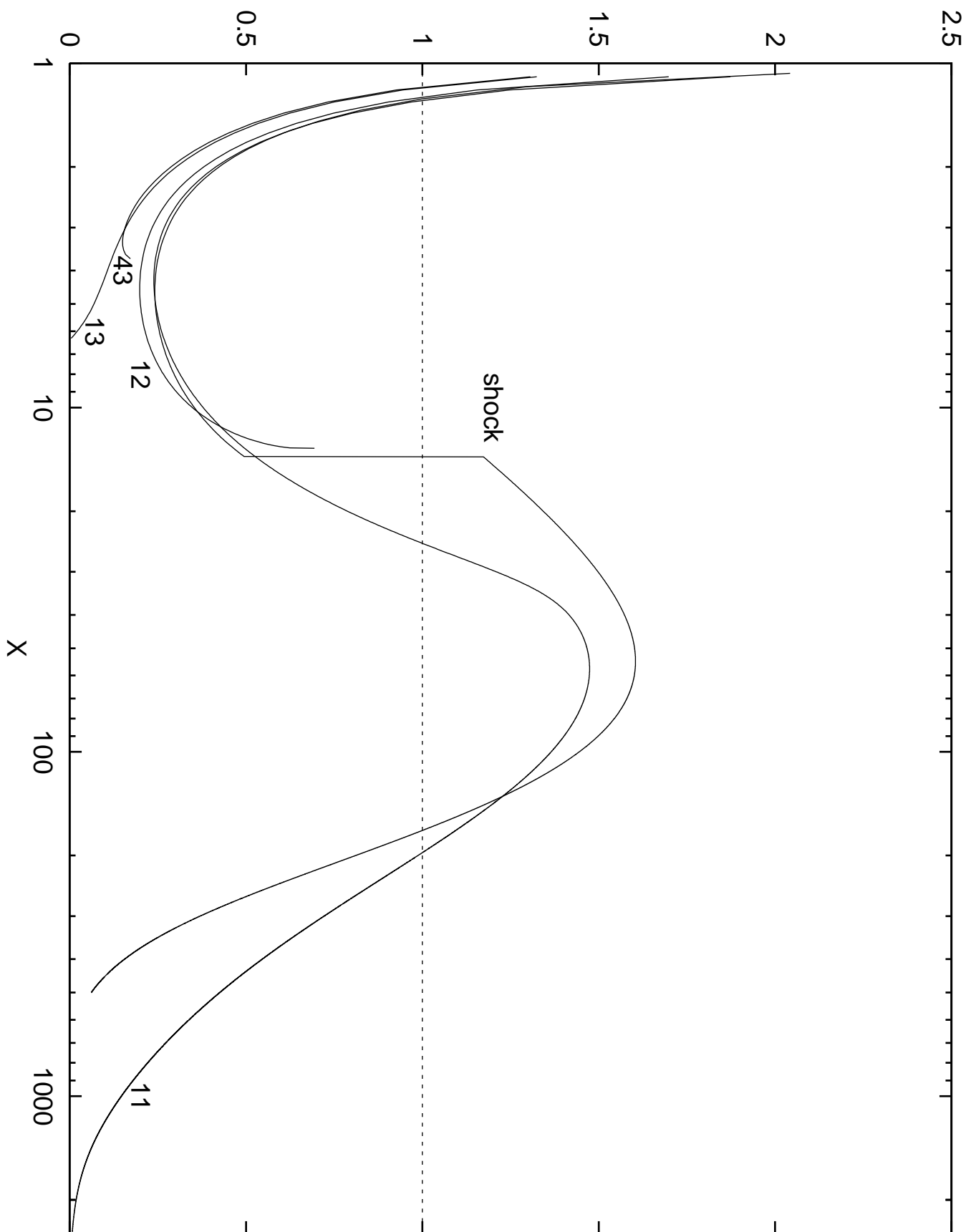


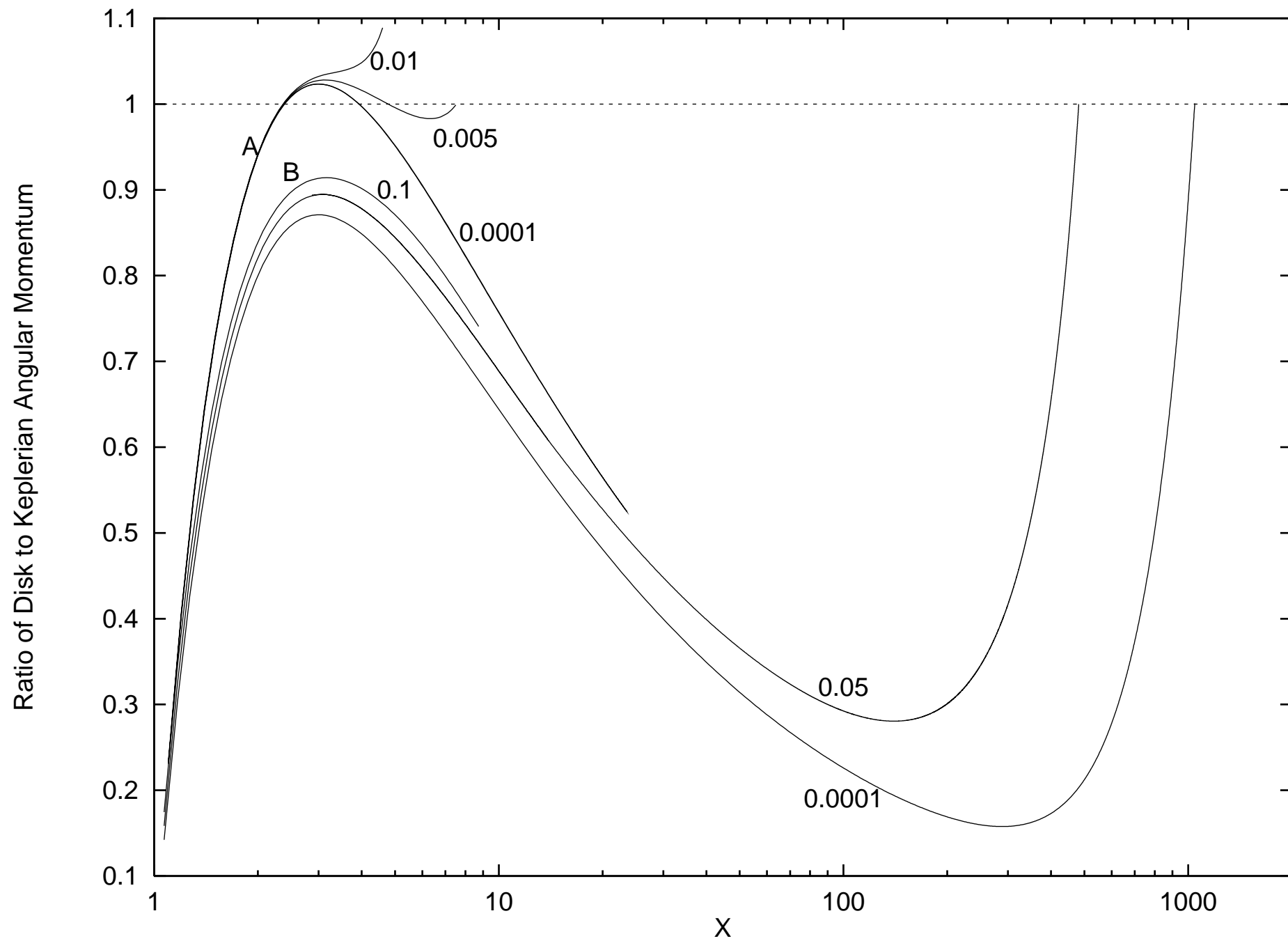


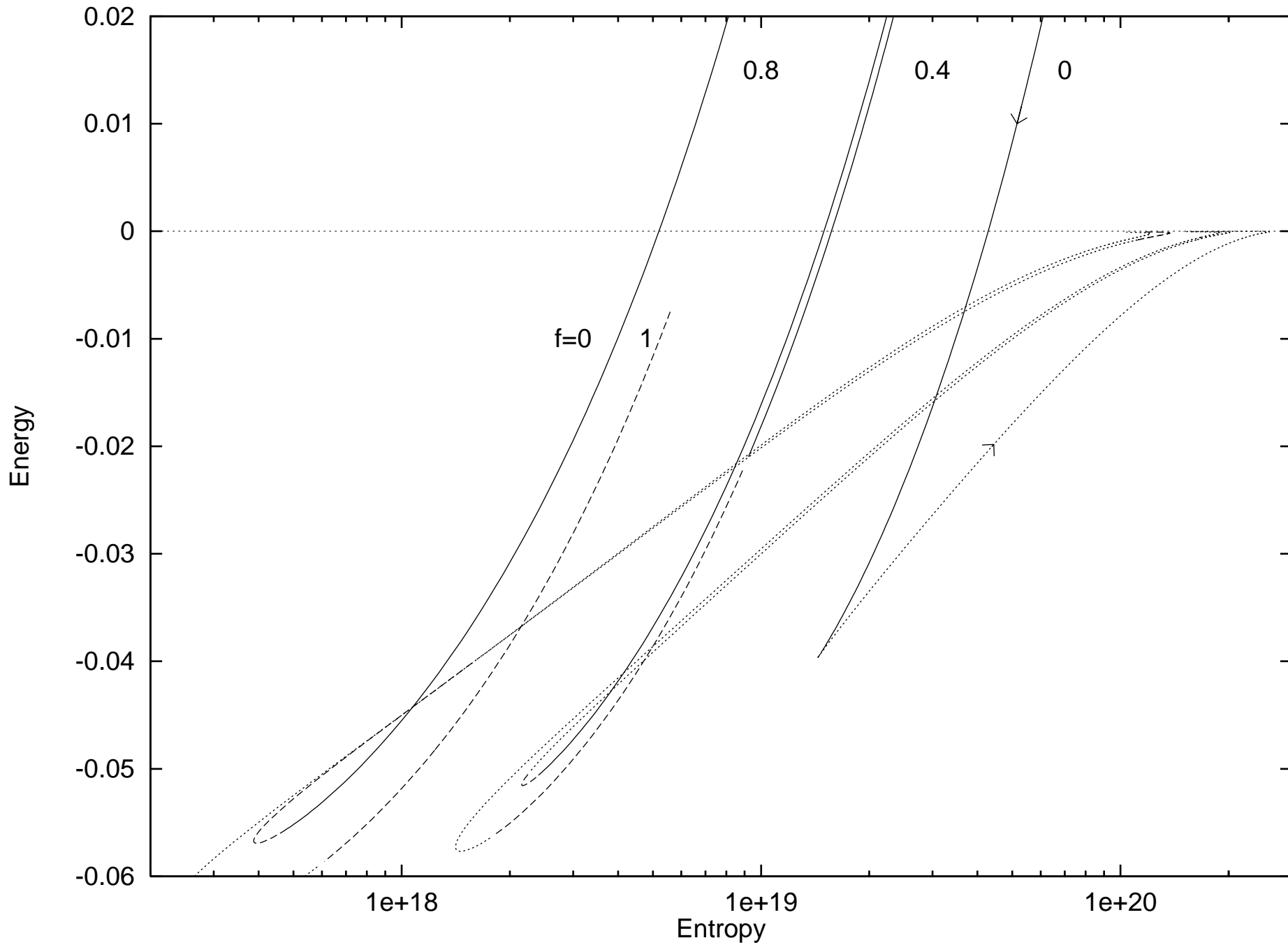




Ratio of Radial and Azimuthal Velocities







2.2

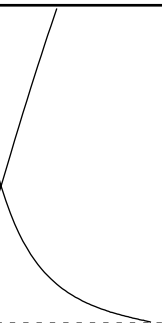
2.5

2.8

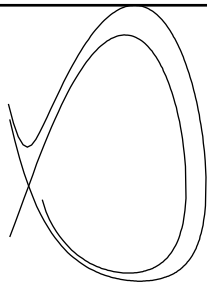
3.1

$f=0$
 $l=1.65$

11



12



13

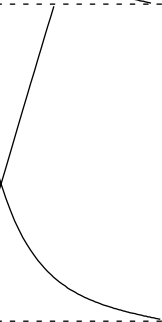


14

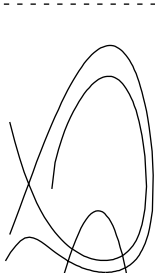
Nodal

$f=1$
 $l=1.65$

21



22



23



24

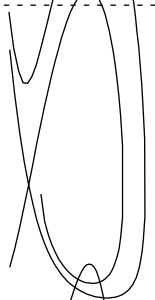
Nodal

$f=0$
 $l=1.8$

31



32



33



34

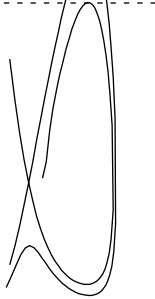
Spiral

$f=1$
 $l=1.8$

41



42



43



44

Spiral

